Characterization of reservoirs, fluids and productions from the Ordovician carbonate condensate field in the Tarim Basin, NW China

Yang, H.[a,b], Wu, G.[a,c], Scarselli, N.[d], Sun, C.[b], Qing, H.[e], Han, J.[b], Zhang, G.[a]

a School of Geoscience and Technology, Southwest Petroleum University, Chengdu, China

b PetroChina Tarim Oilfield Company, Korla, China

c Division of Key Laboratory of Carbonate Reservoirs, China National Petroleum Corporation, Chengdu, China

d Department of Earth Sciences, Royal Holloway University of London, Egham, United Kingdom

e Department of Geology, University of Regina, Regina, SK, Canada

ABSTRACT

TZ-Nº1 Gasfield in the Tarim Basin is the largest condensate field in China, however, it has not developed efficiently because of low and unpredictable production during the past 20 years. Cores, logging interpretation, seismic descriptions, fluid properties and production data indicate that this Ordovician carbonate field is different from conventional stratigraphic oil and gas fields: (1) the hydrocarbon-bearing area covers a large region of 2000 km^2; (2) matrix reservoirs have low porosity (< 6%) and low permeability (< 1 mD) and small throat radii (< 1 μm), but superimposed

fracture-caves with high porosity and permeability are present, resulting in strong lateral poro-perm heterogeneity; (3) significant variations in fluid properties and phases, as well as the absence of a uniform oil-water contact; (4) except for some "sweet spots" in large fracture-caves, production is facilitated by acid fracturing and horizontal drilling, yet there are many low production wells with complex output of oil, gas and water; and (5) more than 70% of the production come from fracture-cave “sweet spots”, but with high decline of production rates (over 20% per year). An examination of the carbonate reservoir and hydrocarbon accumulation history suggests that this large-scale stratigraphic accumulation formed during hydrocarbon emplacement in the Early Paleozoic, with the reservoirs gradually evolving into tight reservoirs as a result of intense diagenesis. Variable amounts of Neogene gas charged the tight carbonate reservoirs and formed unconventional accumulations. TZ-N^{o}1 Gasfield is characterized by a strongly heterogeneous tight matrix reservoir with superimposed fracture-cave reservoir, and complicated unconventional fluid distribution, which provides insights into the exploitation challenges of unconventional carbonate resources.

Key words: Tarim Basin; carbonate reservoir; fluid; oil and gas accumulation; production

INTRODUCTION

Unconventional reservoirs in tight sandstones, coals and shales generally display

low values of porosity (< 10%) and permeability (<1 mD) (e.g., Holditch, 2006; Bruna et al., 2013; Zou et al., 2013). In recent years, with the rapid development of unconventional reservoirs in clastic rocks (e.g., Law and Curtis, 2002; Shanley et al., 2004; Nelson, 2009; Javadpour et al., 2009; Amann-Hildenbrand et al., 2012; Arthur and Cole, 2014; Chew, 2014), unconventional carbonate reservoirs have attracted much attention (e.g., Bruna et al., 2013; Zou et al., 2013; Rashid et al., 2015, 2017; Hakami et al., 2016; Al-Ameri and Gamadi, 2019). Large amounts of hydrocarbon resources could be produced from microporous and fractured tight carbonate rocks with low petrophysical properties (e.g., Zou et al., 2013; Chew, 2014; Rashid et al., 2015; Wei et al., 2017). They are quite different from conventional reservoirs with regard to the state of hydrocarbons, nature of the triple porosity, particularly the technologies required to extract the oil and gas (e.g., Zou, et al., 2010, 2013; Islam, 2015; Al-Ameri and Gamadi, 2019).

Generally, two basic gas reservoir types can occur in sedimentary basins: deep basin gas reservoirs and tight conventional gas reservoirs (e.g., Shanley et al., 2004; Jiang et al., 2006). The former occurs when gas charge post-dates reservoirs tightening, whereas in the latter accumulation of gas predates reservoir tightening (e.g., Jiang et al., 2006; Wang et al., 2014). The time relationship between the emplacement of hydrocarbons and reduction of reservoir porosity is helpful to understand how oil and gas accumulate in these carbonate reservoirs. Some studies on the porosity and pore structure have recorded the complicated processes of the diagenesis and fractures in

tight carbonate reservoirs (Volery et al., 2010; Garland et al., 2012; Bruna et al., 2013; Rashid et al., 2015, 2017; Hakami et al., 2016), while there is little information about the relationship between porosity evolution (mostly porosity reduction) of carbonate reservoirs and hydrocarbon emplacement. This is vital to the identification of unconventionally trapped resources and understand the mechanisms of hydrocarbon accumulation in tight carbonate reservoirs (Shanley et al., 2004; Zou et al., 2013).

In the last two decades, carbonate reservoirs have become a significant frontier in China, including its largest condensate field, TZ-Nº1 Gasfield (Figure 1A), located in the Tarim Basin (Zhou et al., 2010). More than 20 TCF of gas reserves have been discovered in the TZ-Nº1 Gasfield in the northern slope of the Central Uplift. Besides the large reef-shoal reservoir of the Upper Ordovician (e.g. Du, 2010), the exploitation of resources has has reached deeper levels – Lower Cambrian dolomite and Lower Ordovician at depth in excess of 7000 m (e.g. Wang et al., 2014). However, most production wells have low and unpredictable production, and conventional methods cannot efficiently exploit the large reserves there available (Zhou et al., 2010; Wang et al., 2014; Wu et al., 2016a). It is debated whether the TZ-Nº1 Gasfield consists of reef-shoal reservoirs (Yang et al., 2007; Zhou et al., 2010; Zhang et al., 2018) or localized fracture-cave reservoirs (Du, 2010; Yang et al., 2013; Wu et al., 2016a). Furthermore, the origin of the complicated fluid distribution has still not been resolved (Zhu et al., 2014; Wu et al., 2016a; Li et al., 2017).

To decipher the origin and evolution of this complex carbonate field and facilitate

its exploitation, the reservoir, fluid and production data of TZ-Nº1 Gasfield are here presented to show the key characteristics of tight matrix reservoirs with associated "sweet spots" of fracture-cave reservoirs, and their fluid distribution. Together with the hydrocarbon emplacement history and reservoir's evolution, a model is proposed that shows how conventional stratigraphic oil accumulations formed before reservoir tightening, and subsequent gas emplacement resulted in a complex distribution of fluids. This study possibly has significant implications for exploitation of similar unconventional carbonate resources in Siberia, Middle East and Caspian (Ronchi et al., 2010; Tankersley et al., 2010; Garland et al., 2012; Burchette, 2012; Rashid et al., 2015, 2017; Al-Ameri and Gamadi, 2019).

GEOLOGICAL SETTING

The Tarim Basin is the largest petroliferous basin in northwest China, covering about 560,000 km^2 (Figure 1A). It comprises a Cenozoic foreland basin superimposed on a Paleozoic-Mesozoic intracratonic basin with multi-stage tectonic evolution (Figure 1B), which were related to the opening and closure of the Tethys oceans in Paleo-Mesozoic and the Indo-Asian collision in the Cenozoic (Jia, 1997; Li et al., 2010; Wu et al., 2016a and the references therein).

The Central Uplift (Tazhong Uplift) is located in the basin center with an area of 22,000 km^2 and sedimentary rock thickness of more than 9,000 m (Fig. 1). In the Cambrian-Early Ordovician, the Tarim craton was surrounded by the Proto-Tethys

Ocean to the south and the Tianshan Ocean to the north (Jia, 1997). A large carbonate platform developed in western Tarim and an inner basin formed in eastern Tarim in an extensional setting (Li et al., 2013; Wu et al., 2016b). Following the Proto-Tethys Ocean subduction from the south (Dong et al., 2018), the uplift activity in the Central Uplift initiated at the end of the Early Ordovician and was intermittently reactivated from the Middle Ordovician to the Late Devonian (Wu et al., 2012). From Carboniferous to Permian, there were widely distributed siliciclastic sediments with interbedded carbonate rocks in the intracratonic basins (Jia, 1997). A large regional uplift phase resulted from the closure of the Tianshan Ocean of the end of Permian (Jia, 1997; Wu et al., 2016a). During the Mesozoic, the Tarim Basin was influenced by the closure of the Paleo-Tethys Ocean to the south (Wu et al., 2016a; Dong et al., 2018 and the references therein). The Jurassic is absent in the Central Uplift, and prominent unconformities formed during the Mesozoic. Due to the Indo-Asian collision that started in the Neogene, the southern and northern foreland basins developed at the periphery of the Tarim terranes, and the platform-basin was deeply buried (Jia, 1997). In the Central Uplift, Carboniferous to Quaternary sediments were deposited on the Lower Paleozoic uplift, following the creation of multiple unconformities, representing multi-stage regional tectonic activity (Fig. 1B； Wu et al., 2012, 2016a; Li et al., 2013). A series of NW–SE and NEE–SWW striking reverse faults and NE–SW striking strike-slip faults developed in Lower Paleozoic in the Central Uplift (Fig. 1A; Wu et al., 2012, 2016b; Li et al., 2013; Neng et al., 2018).

In excess of 3,000 m of platform carbonates of Cambrian–Middle Ordovician were deposited in the Central Uplift (Li et al., 2010; Gao et al., 2015; Wu et al., 2016a). This succession is composed of thick Cambrian dolomite transitioning to Upper Ordovician limestones (Gao et al., 2014; Gao et al., 2015). A carbonate platform facies of the Lianglitage Formation (Upper Ordovician) formed in the paleouplift regions; this changes laterally to a basinal mudstone facies (Figure 1B; Wu et al., 2016b). The Lianglitage Formation consists of reef-shoal facies in the platform margin, carbonate sand shoal facies and oncoid shoal of open platforms, and lagoon and tidal flat facies in the platform interior (Gao et al., 2014). The reef-shoal facies have 3–5 cycles of shallowing-upward reefs in the steep platform margin along the northern edge of the TZ-Nº1 fault zone (Wang et al., 2008; Zhang et al., 2018). After a short hiatus (Li et al., 2010; Wu et al., 2016a), the thick shelf mudstones of the Upper Ordovician Sangtamu Formation were deposited on the carbonate platform sediments of the Lianglitage Formation (Rong et al., 2013; Wu et al., 2016b).

In the Central Uplift, hydrocarbons are produced in a number of layers from the Cambrian–Ordovician carbonate and Silurian–Carboniferous siliciclastic rocks (Wu et al., 2016a). One of the major reservoir-seal assemblages is the Lianglitage carbonates-Sangtamu mudstones of the upper Ordovician throughout the basin (Figure 1B and 2). The mudstone of the Sangtamu Formation is a favorable regional top seal with a thickness of 200-800 m. Along the No1 fault zone, the Lianglitage Formation consists of 300-500 m thick platform margin limestones occurring at present-day

depths of 4000-7500 m. Two sets of source rocks from the Lower-Middle Cambrian and the Middle-Upper Ordovician have been documented in the Central Uplift (Figure 3; Cai et al., 2009; Li et al., 2010; Yu et al., 2012; Qiu et al., 2012; Zhang et al., 2014; Li et al., 2015; Wu et al., 2016a). Recent studies support that the main source rocks are the Lower-Middle Cambrian strata (Cai et al., 2009, 2015, 2016; Li et al., 2015; Pang et al., 2016), although there is still controversy on the effective contribution of two. Three major stages of hydrocarbon accumulation have been postulated: oil accumulation in the late Caledonian (Ordovician-Silurian) and late Hercynian (Permian), and gas charge in the late Himalayan period (Neogene) (Figure 3; Li et al., 2010; Zhang et al., 2012; Pang et al., 2012, 2013; Liu et al., 2013; Wu et al., 2016a).

METHODOLOGY

6000 km^2 of 3D seismic data have been acquired in the northern part of the Central Uplift, which greatly supported the prediction and identification of carbonate reservoirs (Zhou et al., 2010; Yang et al., 2013; Wu et al., 2016a). More than 100 wells penetrated the Upper Ordovician carbonate rocks of the TZ-N^{o}1 Gasfield, providing substantial amount of core samples, well log data, and production data.

Cores and thin sections from more than 30 wells were compiled to describe pore space and statistics on fractures, pores (diameter < 2 mm) and vugs (diameter between 2–100 mm), as well as lithologies and microfacies (Zhou et al., 2010; Du, 2010; Gao et al., 2014). Core plugs were systematically sampled at a space of 4/m. The porosity

and permeability were measured by liquid saturation method and gas measurement method with klinkenberg-correction, respectively (Du, 2010; Zhang et al., 2018). Well log data were utilized to measure porosity including pores, vugs and caves (cave diameter > 100 mm, large cave diameter > 1000 mm; Wu et al., 2016b) mainly by interpretation of density log data, and fracture porosity derived from dual-lateral log interpretation model (Du, 2010; Tian et al., 2019). The matrix permeability was interpreted using an empirical equation from the matrix porosity-permeability plots of core plugs data (Liu et al., 2009; Du, 2010). Logging interpretation data of about 30 wells were analysed for reservoir classification and correlation of production intervals. In addition, permeability from production tests using pressure decline method (Sivey and Lee, 2013; Wan et al., 2018), and pore-throat radius using mercury intrusion method were statistically analyzed (Wu et al., 2013). Together with physical properties from core plugs and interpreted logs, reservoir correlations amongst wells are presented. Seismic facies and attributes were helpful for sedimentary facies analysis and carbonate reservoir descriptions (Wu et al., 2016a).

Hydrocarbon samples, temperature and pressure data from 24 wells were also compiled. The PVT (pressure–volume–temperature) data proved effective in the identification of fluid phase (Walsh and Towler, 1995; Du, 2010). DST (drill stem test) and acid fracturing data of more than 30 wells were also screened. Aside from the reservoir static data, the dynamic data on oil/gas/water production and pressure changes were used for reservoir and fluid analysis. In this way, all the data pertaining

to unstable fluid production and fluid property changes were screened to identify oil-gas distribution and pool type.

RESERVOIR CHARACTERISTICS

Lithology and facies

The target stratum of the Upper Ordovician Lianglitage Formation is mainly reef-shoal facies along the uplifted edge of the northern platform margin (Figure 1B; Wang et al., 2008; Gao et al., 2014). This is a multicyclic assemblage of reefs and shoals (Liu et al., 2012; Qu et al., 2013; Gao et al., 2014), following episodic subsidence and sea level fluctuations (Wu et al., 2016a). Reefs comprise massive receptaculitids porifera framestone, stromatoporoid framestone, coral framestone, algae binding bioclastic limestone, and algae binding psepholite limestone (Figures 4A-D; Wang et al., 2008; Gao et al., 2014; Gao et al., 2015; Wu et al., 2016a). Single reefs are small, measuring ~cm to ~m thick in cores. The shoal facies includes bioclastic shoals and carbonate sand shoals that are rich in grainstones (Figures 4D, 4E), and interbedded with small reefs and mudstones. Reef facies mainly developed in the eastern area, but are interbedded with bioclastic shoals and carbonate sand shoals in the central and western Nº1 fault zone (Wang et al., 2007; Gao et al., 2014). The lithology of the reef-shoal facies changed frequently both vertically and laterally (Figure 5). Therefore, it is difficult to correlate lithology between wells, particularly the reef bodies. Seismic profiles through the reef-shoal complexes often show these

being mound-shaped (Figure 6). The shoals are not limited to the platform margin but are distributed widely in the backreef zone of the inner platform (Wu et al., 2016a; Zhang et al., 2018), despite rapidly decreasing interval thickness and size of grainstones.

Lithology and facies correlation (Wang et al., 2007; Zhang et al., 2018) together with 3D seismic analysis (Wu et al., 2016a) has allowed to map a large-scale reef-shoal complex that developed along a platform margin with a length up to 220 km, a width of 2-8 km extending over an area of ~800 km^2 (Figure 6). This is consistent with a steep and narrow paleogeomorphology at the northern edge of the Central Uplift (Gao et al., 2014; Gao et al., 2015; Wu et al., 2016b). It is noteworthy that the platform margin is wider in the west and narrower to the east, thicker to the north and thinning towards the south (Figure 6).

Reservoir

The carbonate reservoirs of the Upper Ordovician Lianglitage Formation are mainly grainstones (Figures 4 and 7A-H; Wang et al., 2007; Du, 2010; Liu et al., 2012; Gao et al., 2014; Wu et al., 2016a). There is strong cementation likely related to a long burial history (Wang et al., 2008; Jia et al., 2016; Zhang et al., 2017), which occluded most primary porosity (Figure 4). Secondary porosity is related to caves, dissolution vugs and pores, and fractures (Du, 2010; Wu et al., 2016a; Zhang et al., 2018).

In cores, dissolution pores and vugs developed in the reef-shoal reservoir (Figures

4F and 7A-H). Generally, the dissolved vugs and pores are rounded or irregular with a diameter of 0.5-3 mm. The porosity is partially filled with multiple cements and shows a surface porosity of up to 9%. Dissolution porosity possibly occurred along bedding plane, forming porous interval with a thickness ranging 0.05-1 m. Although some residual and dissolution porosity occurred in the reef limestones (Wang et al., 2008), they are too scattered to form thick porosity intervals (Figure 4A-D). In thin sections (Figures 4E-F, 7D-H), most primary pores are cemented and replaced by secondary dissolution pores, mainly intergranular dissolution pores and partial microfracture (aperture < 10 μm) and intragranular pores. Intergranular dissolution pores are common in thin sections and contribute to more than 80% of porosity. Most pores in the grainstones are irregular with varied size, and with a diameter ranging 0.01-1 mm. Intragranular pores are generally residual micropores (diameter < 10 μm) in reef limestones, and dissolution micropores in large grainstones (Figures 4F and 7D). Intragranular pores are small, with diameters of 0.01-0.3 mm.

High angle fractures developed in the rock with narrow aperture of < 0.5 mm (Figures 7B-C). In addition, the dissolved pores and vugs along fractures are common. Multistage cementation and dissolution along the fractures suggest multiple phases of fracture reactivations (Ding et al., 2012; Wu et al., 2016a) with most partially filled by calcites. This is consistent with synchronous fracturing and fluid flow activity in the Ordovician carbonates (Wu et al., 2016a; Zhang et al., 2017).

Some wells penetrated into caves and suffered from large amounts of mud loss,

abnormal drilling breaks, and mud overflow during drilling process (Du, 2010; Ni et al., 2013; Yang et al., 2013; Wu et al., 2016a, 2016b). Examples include mud loss reaching 799.2.5 m^3 and two intervals of drilling break with thicknesses of 0.2 m and 0.5 m in well TZ62-1. The typical log characteristics of caves are: significantly enlarged borehole diameter, increased natural gamma, and decreased resistivity (Figure 7J; Ni et al., 2013; Wu et al., 2016a; Tian et al., 2019). Notably, "bead-shaped" strong reflections (low frequency and strong amplitude reflection of wave crest and trough in seismic profile) in seismic profiles are generally interpreted as the response of large caves (Figure 7K; Du, 2010; Yang et al., 2013). Most "bead-shaped" reflections are proved to be large cave intervals by log and production data, and are generally assumed to be extensive fracture-cave reservoirs (Du, 2010; Ni et al., 2013; Yang et al., 2013; Wu et al., 2016a).

The pore structure has a complicated irregular size related to the multistage cementation-dissolution nature of the pores (Wu et al., 2013). Most of the pore throats are micro-throats (radii < 0.1 μm), even in large pores (Figure 7I). Although filled by cements, fractures generally have big pore throats (radii > 10 μm) that are different from the matrix porosity (Figures 7G, 7H). The majority of the pores are tiny and complex in shape, with a few well connected by fracture. The statistics of throat radius without fracture samples show that the average throat radius is generally less than 1 μm.

Reservoir porosity and permeability

Statistical analysis of core plugs measurements (Figure 8A) indicates that the porosity ranges 0.1-10.1%, with an average porosity of 2.2%. The permeability values vary widely between 0.008–516 mD, mostly with permeability lower than 1 mD and few cases lower than 0.1 mD. It is noteworthy that permeability values >1 mD are mainly from the fracture-bearing samples. Despite the lack of a correlation between the porosity and permeability in the dataset (Wang et al., 2008; Wu et al., 2016a), there is a good correlation between porosity and permeability from the oil-bearing samples without fractures, as determined through the full diameter core test. The porosity from well log interpretation usually ranges from 1.2- 8%, and the permeability varies over a large range of 0.01-100 mD (Figure 8B). Except for the fractured zones, the matrix reef-shoal reservoirs represent extremely low permeability to tight reservoirs. In addition, the permeability can increase 10–100 times in the fracture zones (Figure 8B). The higher permeability intervals (>1 mD) are almost all fracture bearing intervals. On the other hand, some intervals with large caves have a porosity in excess of 10% (Figure 7J; as determined by log data) despite being filled with breccia, calcite, and others minerals (Qu et al., 2013; Wu et al., 2016b).

Core plugs analysis indicates that bioclastic limestones, biocalcarenite and sparry calcarenites have better matrix reservoirs (Table 1). The mudstones generally have low porosity (< 1%) and low permeability (< 0.7 mD). Good reservoirs are generally grainstones in the reef flank and bioclastic shoal, followed by carbonate sand shoal

facies. The reservoirs are well developed in the reef base–reef limbs and bioclastic shoals, with an average matrix porosity of 2-5%.

Table1 the porosity and permeability of the reef-shoal reservoirs

lithology	porosity（%）		permeability（mD）	
	range	average	range	Average
bioclastic limestone	3.57–1.13	1.8	9.52–0.04	1.74
biocalcarenite	4.60–0.01	1.6925	6.44–0.007	0.6325
sparry calcarenite	5.9–0.01	1.5075	8.94–0.003	0.3075
bondstone-framstone	5.0–0.5	1.145	1–0.02	0.27
micrite calcarenite	7.16–0.05	1.076	8.53–0.01	0.766
mudstone	5.07–0.05	0.9625	9.52–0.012	0.725
algal mudstone	7.54–0.27	0.9475	8.53–0.004	0.6325

(523 core plug samples; the bioclastic limestones, biocalcarenite and sparry calcarenites are mainly grainstones. The bondstone-framestone belongs to reefs, and the micrite calcarenite can be classified as packstone-wackstone. This classification scheme is particularly relevant for thin section analysis – see Du, 2010).

Reservoir distribution

Based on log data, a favorable reservoir interval is located in the upper 100 m of the Lianglitage Formation (Figures 2 and 5; Wang et al., 2007; Wu et al., 2016a). The effective reservoir thickness is about 30–70 m, with the thickness of a single layer ranging from 2–6 m. Log interpretation (Figure 5) suggests that the reservoirs are

weakly connected and laterally vary in thickness and in physical properties. In places, these reservoirs are formed by fracture-caves superposed vertically, and where overlapping, they form large areas of the otherwise poor quality tight carbonate reservoirs (Du, 2010; Zhang et al., 2018).

Seismic mapping shows that the reef-shoal reservoirs are widely distributed along the platform margin and are heterogeneous (Figure 9), becoming tight progressively toward the inner platform. However, there are still good reservoirs in the inner zone as well as poor reservoirs along the margin (Zhang et al., 2018). This is consistent with production data. Large caves are localized in restricted areas and form less than 5% of the total reservoir in term of lateral extent (Du, 2010; Wu et al., 2016a).

FLUID AND PRODUCTION OUTPUT

Fluid property

Multiple hydrocarbon phases (i.e. bitumen, heavy oil, normal oil and light oil, wet gas and dry gas) are found in the Ordovician carbonates. In the study area, fluid samples show significantly variable properties (Figures 10-12; Du, 2010; Wu et al., 2016a; Li and Cai, 2017).

Oil properties varied amongst wells (Figure 10). The density of surface crude oil varies from 0.78-0.87 g/cm^3 (20 °C), with the oil characterized as a combination of condensate and normal oils. Crude oil viscosity is 0.8847–8.117 mPa•s (50 °C); freezing point is from 18–16 °C; average sulfur is 0.06-0.5%; and wax content is

1.25-16.08% (Du, 2010; Wu et al., 2016a). Generally, crude oil has low density, low viscosity, minimal sulfur, and middle–low wax content. However, some wells have oil with high density, middle–high wax content, and high sulfur, suggesting the complexity of oil accumulation and alteration (Cai et al., 2009, 2016; Zhu et al., 2014; Li et al., 2014).

The gas components (Figure 11) include CH_4 (66.1–95.98%), CO_2 (0.1381–5.08%) and N_2 (2.27–16.34%). The average density is 0.75-1.14 g/l. H_2S is commonly present in this area with a broad range of 0–23,600 ppm. Except for some dissolved gas in the oil production wells, the samples display dry gas with a high dryness coefficient of more than 0.95. Notably, the dry gas coexists with normal oil with a density of up to 0.85 g/cm^3 even in a well. The dry gas is possibly of late emplacement, during the Eocene (Du, 2010; Wang et al., 2014; Zhu et al., 2014; Wu et al., 2016a).

The GOR (gas/oil ratio) varies from 0-2,600 m^3/m^3, with most exceeding 1,000 m^3/m^3 (Figure 10). Whereas, GOR is less than 600 m^3/m^3 with high oil density in several wells in the gas field. The PVT analysis of most samples reveals condensate gas that appears in a single gas phase as a medium–high condensate (Figure 12). The little difference between the formation pressure and dew point pressure indicates that oil saturation is close to the critical value. However, a few wells (e.g. well T62-1) show weak volatile or high saturation oil, which are inconsistent with the peripheral condensate gas (Figure 10).

The formation water is $CaCl_2$-type water, with average density at 1.01-1.09 g/cm^3 and the total salinity at approximately 62,340-137,900 ppm. These values show large differences in formation water in the same well area, suggesting the absence of a uniform oil-gas-water contact. The formation water cut in the platform margin is less than that in other areas (Du, 2010; Wu et al., 2016a).

The temperature gradient obtained in the regression analysis is about 2.15 °C/100 m from the well bottom temperature data, indicating a uniformly low geothermal gradient. The formation pressure coefficients vary in a large range of 1.13–1.26, suggesting normal pressure and slightly abnormal high pressure coexisting along the platform margin.

Oil, gas and water production

All but one of the over 50 wells had oil or gas production, while along the platform margin more than 80% of the wells had very low production as revealed by DST data (Figure 13). In order to achieve commercial exploitation of these carbonate reservoirs, unconventional techniques, such as large acid fracturing and horizontal well drilling, have been widely used.

Except for several highly productive wells targeting large caves, most wells have low yield, even after fracturing (Figure 13). Following acid fracturing, about 80% of the wells obtained higher production, but some wells were still unable to gain commercial production. High production though was attained immediately after

large-scale acid fracturing and production declined soon after. Currently, more than one-third of the wells still could not provide commercial production.

Horizontal drilling technology has also been used in wells targeting the matrix reservoirs facies. Horizontal penetration can be in excess of 1400 m and typically reach a number of fracture-vug intervals. With the combination of multistage acid fracturing, production is stable and can be more than five times greater than for vertical wells. However, production data also show a quick production decline in many wells (Du, 2010; Wu et al., 2016a), suggesting a low permeability of the reef-shoal reservoirs. For example, well TZ62 has a high matrix porosity reservoir (Figure 14A; Wu, 2016a). It recorded a low production at 1 bbl/d through DST, but a high oil and gas production following acid fracturing of 240 bbl/d and 1070 mcf/d, respectively. In the pre-production phase, the initial daily average oil production was 115-140 bbl, and the daily gas production was 570-820 mcf. One year later, the daily production decreased to 60 bbl/d of oil, following a fluctuated production of gas and water. In this area, most wells with initial high production declined in a short time (< 1 year). In addition, many wells had periodical variation of production (Figure 14B), with several wells suddenly increasing their output during the production period. This scenario suggests an unstable production from the carbonate reservoirs likely related to extreme heterogeneity and complex connectivity in the reservoir units (Wu et al., 2016a).

There is limited water production in most reef-shoal reservoirs, although some

fracture-cave reservoirs had fast water flooding during production. Water production was also unstable, showing a slow increase with unpredictable variation, and periodic phases of decrease (Figure 14). The water/oil ratio varies unpredictably across the field. This indicates that the edge water or bottom water are inactive in most of the reservoirs, and there is a much lower water ratio than in the northern Tarim basin (Du, 2010). It is noted that some wells with high water production are located on a structural high, whereas wells with high hydrocarbon production are located in nearby lows.

In addition, the gas/oil ratio and oil density vary during production, following intermittent cycles of decrease or increase. Even in the same well, fluid properties may vary during production. The oil density changed from 0.79-0.85 g/cm^3, and the gas/oil ratio of 2,000 m^3/m^3 decreased to about 500 m^3/m^3 in well T622 after one year of pre-production (Figure 15). This suggests different fluid flows from different compartments, as well as variation in fluid phase from condensate gas to normal oil.

Currently, unpredictable production and complicated water flooding are the key challenges in the exploitation of these carbonate reserves (Figures 14). Because of these challenges, more than 30% of the wells cannot be put into production, and many wells have low production during the initial production period. In the dataset, 30% of the wells that penetrated the fracture-cave 'sweet spots' provided stable oil and gas output and form about 70% of the production. Production typically has a rapid decline rate of more than 20%, and stable production from a well commonly does not last for

more than 6 years. The estimated recovery ratio for oil and gas is generally less than 20% and 50%, respectively.

DISCUSSION

Reservoir types

From the core samples and well log data (Figures 8A and 8B), most matrix reservoirs have low porosity (< 6%) and low permeability (< 1 mD). The high permeability values (> 1 mD) are typically related to the presence of pervasive fractures. Together with low pore throat radius (< 1 μm), the matrix carbonate reservoirs in the Tarim Basin can be compared with tight sandstones (Shanley et al., 2004; Nelson, 2009). In the deep subsurface, many oil or gas bearing intervals show extremely low formation permeability (less than 0.1 mD; Figure 8C), which is consistent with little DST output. The permeability of matrix reservoirs decreases from core plugs to production zones, possibly resulting from weak reservoir connectivity (Wu et al., 2016a). It is noted that low production occurred in many DST intervals with low permeability (relative tight reservoirs; permeability < 5 mD) as well as some fractured reservoirs. In addition, many matrix reservoirs only exhibited low production even when facilitated with large acid fracturing (Figure 13).

The permeability in fractured reservoirs is 1–2 orders of magnitude larger than for the matrix reservoirs (Figure 8A, 8B). Most of the high production intervals are affected by fractures, and are found within fault damage zones in the close proximity

434 to large faults. Thus, fractures play an important role in the heterogeneity and
435 production of the carbonate reservoirs (Wu et al., 2016b). It is noted that the "sweet
436 spots" in the fracture-cave reservoirs support most of the commercial production in the
437 Central Uplift. However, the "sweet spots" are scattered within the field (< 10% of the
438 areal extent of the reservoir) and form < 5% of the logged reservoir intervals (Du,
439 2010; Yang et al., 2013; Wu et al., 2016a).

440 The superposition of fractures and caves also lead to intense heterogeneity of the
441 carbonate reservoirs (Figures 5 and 7). The strong heterogeneity of tight matrix
442 reservoirs (permeability < 1 mD) with exceptionally high permeability
443 fracture-caves (> 10 mD) are quite different from typical tight carbonate reservoirs,
444 such as the tight Carboniferous carbonate in the Pre-Caspian basin (Ronchi et al., 2010;
445 Zou et al., 2013; He et al., 2014). In the Tengiz carbonate field, there is generally
446 residual primary porosity and high matrix porosity, more than 6% in the tight
447 carbonate reservoirs, with some well-developed fracture porosity (about 0.4%)
448 (Tankersley et al., 2010; Ronchi et al., 2010; He et al., 2014).

449 In addition, the physical properties of the fluids are quite different among the
450 wells in the Tarim Basin (Figures 10-12), with condensate gas mixed with oil, wet gas
451 and dry gas present. These present a more complicated fluid distribution than other
452 tight carbonate reservoirs (e.g., Bruna et al., 2013; Zou et al., 2013; He et al., 2014),
453 such as the Turonian–Campanian Kometan Formation in northern Iraq (Rashid et al.,
454 2015) and Jurassic Tuwaiq Mountain Formation in Saudi Arabia (Hakami et al., 2016).

455 The exploitation is also hindered by the periodic and unstable nature of production
456 (Figures 14), and varied fluid output during the production (Figure 15). The
457 complicated fluid distribution in the Ordovician carbonate reservoirs shares some
458 similarities with the unconventional reservoirs controlled by non-Darcy flow (Law and
459 Curtis, 2002; Amann-Hildenbrand et al., 2012; Zou et al., 2013; Islam, 2015).
460
461 **Reservoir evolution**
462 Carbonate reservoirs are generally influenced by depositional microfacies and
463 fabrics, and diagenetic alteration (Choquette and Pray, 1970; Esteban and Taberner,
464 2003; Moore and Wade, 2013). During the long and complex tectono-diagenetic
465 evolution of the Upper Ordovician carbonate of the Tarim Basin (Figure 16), these
466 reservoirs have undergone multiple phases of porosity loss and enhancement. There is
467 much controversy on the factors that microfacies can influence the poro-perm
468 characteristic of the carbonate reservoirs (Wang et al., 2007; Liu et al., 2012; Wu et al.,
469 2016a). Various diagenetic factors are proposed such as penecontemporaneous
470 (immediately after the deposition) dissolution (Liu et al., 2012; Shen et al., 2015),
471 hydrothermal dissolution (Cai et al., 2008; Pan et al., 2009; Yang et al., 2012; Jiang et
472 al., 2015), TSR (thermochemical sulfate reduction) (Cai et al., 2001; Li et al., 2014)
473 and subaerial karstification (Qu et al., 2013; Wu et al., 2016b), or various
474 combinations of these (Wang et al., 2007; Du, 2010; Shen et al., 2015).
475 Most of the Upper Ordovician carbonate reservoirs presented in this study are

reef-shoal facies and carbonate sand shoal facies in a platform margin (Wang et al., 2007; Gao et al., 2014), with their sedimentary characteristics controlling reservoir quality (Wang et al., 2008; Liu et al., 2012; Shen et al., 2015; Zhang et al., 2018). Good reservoirs are generally grainstones in the reef flank and bioclastic shoal, and then the carbonate sand shoal facies (Table 1; Wang et al., 2007), suggesting that the lithology and facies has an influence on porosity formation and preservation. This is consistent with large amount of oil resources found in these matrix reservoirs (Du., 2010).

Penecontemporaneous dissolution from meteoric water may have improved the matrix porosity (Du, 2010; Shen et al., 2015), while secondary dissolution porosity of the Ordovician carbonate generally formed during burial (Cai et al., 2001; Wang et al., 2008; Yang et al., 2012; Zhang et al., 2017). Secondary porosity is related to meteoric water, mixing water and hydrothermal fluid (Qu et al., 2013; Jiang et al., 2015; Jia et al. 2016; Zhang et al., 2017). At least five stages of dissolution of skeletal allochems or cements are identified (Zhang et al., 2017). However, there are still uncertainties related to the driving mechanism for generation and preservation of secondary porosity in these deeply buried carbonates (Ehrenberg et al., 2012; Zhang et al., 2017). Secondary porosity may have increased by: (1) carbon dioxide and organic acids following the oil or gas accumulation during the Early Paleozoic, Late Paleozoic and Neogene (Wang et al., 2008); (2) hydrothermal dissolution during Permian magmatism (Pan et al., 2009; Yang et al., 2012; Jiang et al., 2014); or (3) TSR during the Neogene

(Li et al., 2014; Jia et al., 2016). However, there is no clear evidence supporting large scale dissolution porosity due to carbon dioxide or organic acids (e.g. Ehrenberg et al., 2012). Some studies proposed strong hydrothermal activity (Cai et al., 2008; Pan et al., 2009; Yang et al., 2012), consistent with the occurrence of LIPs (large igneous provinces) during the Permian (Jia, 1997; Wu et al., 2016a), which may have played a role in the development of caves and vugs in the Ordovician reservoirs (Pan et al., 2009; Yang et al., 2012; Jia et al., 2016). Cai et al. (2008) argued against igneous activity as the source of hydrothermal fluid, which needs further study. Hydrothermal dissolution could be a viable mechanism for dissolution of deeply buried reservoirs near fault zones; whereas secondary porosity formed in one place generally are followed by a filling process in another place by dissolution mass transport in a close system (Davies and Smith, 2006; Ehrenberg et al., 2012). In this context, it is possible that hydrothermal minerals, such as calcite and fluorite, occluded the porosity in the carbonate vugs rather than increasing the porosity of these reservoirs. TSR redox reactions between petroleum and sulfates at temperatures higher than about 120 °C, has been proposed to occur in the Neogene (Cai et al., 2001; 2016; Li et al., 2014; Jia et al., 2016). The TSR may favor burial dissolution of dolostones (Cai et al., 2014; Guo et al., 2016), but this study indicates that the related porosity enhancement is limited in the limestones. It is noteworthy that most of dissolution porosity is associated with the faults and fractures (Wu et al., 2016a, 2016b), suggesting an important role of fracturing in enhancing secondary porosity.

518 Recent studies indicate that meteoric karstification provide a mechanism for the
519 creation of large fracture-cave reservoirs – the “sweet spots” in the Ordovician
520 carbonate reservoirs of the study area (Qu et al., 2013; Wu et al., 2016b). New seismic
521 data and borehole data identified an unconformity on the top of the Ordovician
522 carbonate in the eastern Nº1 fault zone (Wu et al., 2016b). Karst features, including
523 karstic rubble, argillaceous fillings, irregularly dissolution ditches and vadose silt
524 fillings, have been identified in the cores (Qu et al., 2013; Wu et al. 2016b). These are
525 compatible with high production wells in the eastern Nº1 fault zone. The
526 superimposed large fracture-caves were possibly formed by karstification in the Late
527 Ordovician, and burial dissolution from the Paleozoic to Neogene (Wang et al., 2007;
528 Wang et al., 2008; Yang et al., 2012; Jiang et al., 2015). In this context, a good matrix
529 reservoir (general porosity > 6% and permeability > 1 mD) still exists in the shallow
530 section to the bottom of the Early Paleozoic (Figure 16). Due to most primary porosity
531 being occluded by cementation in the Paleozoic (Du, 2010; Yu et al., 2015; Zhang et
532 al., 2017), the tight matrix reservoir possibly formed before the Mesozoic. During
533 their long burial history, the Ordovician carbonate reservoirs have undergone
534 multistage diagenesis, followed by dissolution that formed multiple secondary
535 porosities and marked heterogeneity, resulting in a complex and peculiar carbonate
536 reservoir (Davies and Smith, 2006; Ronchi et al., 2010; Ehrenberg et al., 2012, Radish
537 et al., 2015).
538

Oil and gas accumulation

Regardless of the debate surrounding key source rocks and timing of hydricarbon accumulation in the study area (e.g., Cai et al., 2009, 2016; Li et al., 2010; Zhang et al., 2012, 2014; Yu et al., 2012; Qiu et al., 2012; Li et al., 2015; Pang et al., 2016), extensive oil emplacement in the late Caledonian (Late Ordovician-Silurian) and late Hercynian (Permian) is assumed to be responsible for the main reserves in the Central Uplift (Figure 3 and 16; Li et al., 2010; Pang et al., 2012, 2013; Liu et al., 2013; Pang et al., 2018). Large accumulations in stratigraphic stratigraphic traps formed along the platform margin and some in the inner zone in Late Ordovician (Figure 17A; Li et al., 2010; Pang et al., 2012; Wu et al., 2016a).

During the long history of post-entrapment, the earlier entrapped hydrocarbons re-adjusted and some escaped in the Central Uplift (Pang et al., 2012; Zhang et al., 2012; Pang et al., 2018). Evidence from bitumen, heavy oil residual and geochemical data suggest a complex alteration process of hydrocarbon reservoirs. All the accumulations found in the inner platform had active water, suggesting that only part of the oil is preserved in the unsaturated accumulations. Furthermore, large reservoirs, and large caves in particular, have high water-cut, indicating extensive oil loss after oil emplacement. The post-entrapment alteration may have different impacts on the composition of the hydrocarbons (Figure 11). The fluid varied with the cap rocks, fault activities and water-flushing-biodegradation (Pang et al., 2012; Wu et al., 2016a). Because of subsequent tectonic events, 70% of the original Ordovician hydrocarbon

accumulation has been lost in the Central Uplift (Pang et al., 2012; Pang et al., 2018).

Previous studies suggested that the reservoirs became tight prior to the Mesozoic (Figure 16) (e.g., Wang et al., 2008; Zhang et al., 2017). Even if the accumulation of the oil and gas can hinder porosity decrease, diagenesis such as compaction, cementation, quartz overgrowth and clay minerals, and tectonic stress can progressively lower the porosity in the low oil and gas saturation reservoirs (e.g., Jiang et al., 2006). The carbonate reservoirs have undergone in situ precipitation and cementation after the Paleozoic accumulation (Wang et al., 2010; Zhang et al., 2017), particularly in low saturation oil and gas reservoirs (Pang et al., 2012, 2013; Pang et al., 2018). In addition, some of the large cave reservoirs display a distinct bottom water (Du, 2010; Pang et al., 2012; Wu et al., 2016a), suggesting conventional oil accumulation by oil-water differentiation (Shanley et al., 2004). These are consistent with hydrocarbon emplacement in the Paleozoic *before the carbonate reservoir tightened*. In these tight reservoirs, gravity differentiation shows weak impact on the fluid differentiation (e.g., Shanley et al., 2004; Nelson, 2009; Rashid et al., 2015, 2017). Thus, the oil was initially charged into stratigraphic traps with uniform properties, but then gradually evolved into varied properties due to post-entrapments adjustment (Figure 17B).

In the late Cenozoic, the matrix reservoirs had been tightened with poor reservoir connectivity during deep burial (Wang et al., 2008; Liu et al., 2012; Shen et al., 2015; Zhang et al., 2017). Gas charging occurred at this time (Li et al., 2010; Wang et al.,

2014; Zhu et al., 2014) as suggested by the inclusion temperatures of 120–150 °C (Figure 16), probably migrating through fault zones into the tight reservoirs (Figure 17C) (Lan et al., 2015; Wu et al., 2016b; Neng et al., 2018). As gas migrated to the southern area into the tight reservoirs, the gas/oil ratio gradually decreased from the lower to the higher positions (Figure 10). The entrapped oil could turn to condensate gas with various properties by the amount of gas charge in the late stage (Wang et al., 2014; Zhu et al., 2014). In addition, some compartments remain as oil reservoirs with weak gas cut resulting from tight barriers. Large amounts of oil in the southern highs suggest that the front of the charging gas has yet to reach these areas (Figure 17C). Furthermore, gas migration may not follow Darcy flow in tight reservoirs with low throat radii (<1 μm) (Wu et al., 2013), and subsequently it may tend to be forced by diffusion without obvious gravity differentiation in tight reservoirs (e.g., Zou et al., 2010, 2013; Islam, 2015). Consequently, the accumulated hydrocarbons are characterized by the absence of total differentiation of uniform gas-oil-water contacts. Considering that the late gas charging is from low to high positions in tight reservoirs (Wu et al., 2016a), this resulted in much more gas enrichment in low positions but more oil in high positions (Figure 17C). Of course, the scattered “sweep spots” of large fracture-cave reservoirs possibly have distinct oil-gas-water contacts.

Implications for carbonate reservoirs exploitation

Tight carbonate reservoirs have recently been found and attracted attention in the

Sichuan and Ordos basins (e.g., Deng et al., 2013; Wei et al., 2017), Caspian (e.g., Tankersley et al., 2010; Zou et al., 2013), Europe (Volery et al., 2010; Bruna et al., 2013) and the Middle East (Ray et al., 2012; Rashid et al., 2015). Low permeability, less than 1 mD and even lower permeability than 0.1 mD (Wei et al., 2017), in the tight carbonate reservoirs is in line with the definition of tight sandstone reservoirs. These tight carbonate reservoirs generally coexist with conventional carbonate reservoirs in mature basins (Kuznetsov, 1997; Ronchi et al., 2010; Garland et al., 2012; Wei et al., 2017; this study). Whereas, in the Tarim Basin, tight carbonate reservoirs are superimposed with fractures and caves, which form secondary porosity, accounting for more than 90% of porosity in the tight carbonate reservoirs and being possibly independent of lithology (e.g., Wu et al., 2013; Hosseini et al., 2018). Multiple diagenetic cycles, particularly burial dissolution, are more complicated to those observed in other places (Esteban and Taberner, 2003; Davies and Smith, 2006; Ronchi et al., 2010; Ehrenberg et al., 2012; Garland et al., 2012; Moore and Wade, 2013). Further, the dissolution related to multiple fracture activities is of significant importance to the heterogeneity in the tight reservoirs (e.g., Ray et al., 2012; Tian et al., 2019; Guo et al., 2019). These need further study to decipher the multiple diagenetic processes and their impacts on carbonate reservoirs.

Technically, the extremely low porosity and permeability, and strong heterogeneity make it difficult to evaluate the effectiveness of tight carbonate reservoirs (e.g., Deng et al., 2013; Li et al., 2018). Nevertheless, conventional models

623 are not satisfactory to interpret multi-scale or in-situ observations (Li et al., 2018).
624 Seismic mapping makes it possible to optimize drilling targets in the fracture-cave
625 "sweet spots" in the Tarim Basin (Yang et al., 2013; Wu et al., 2016a). However, there
626 is still a challenging task for geoscientists and geophysicist, which is to enhance
627 production from these tight carbonate reservoirs (Rashid et al., 2015, 2017; Wu et al.,
628 2016a). Horizontal well drilling and multiple cycles of acid fracturing have been
629 implemented to stimulate the tight carbonate reservoirs in the Tarim Basin (Du, 2010),
630 while much work is needed to optimize acid fracturing design (Guo et al., 2019;
631 Al-Ameri and Gamadi, 2019), as well as understanding the 'producibility' issues in
632 these tight carbonates (Burchette, 2012).
633
634 **CONCLUSIONS**
635 In the Tarim Basin, the Ordovician carbonate reservoirs and the hydrocarbons
636 found in these units form a complex unconventional resource highlighted by the
637 following characteristics:
638 1. The carbonate reservoirs are formed by tight matrix reservoirs (porosity < 6%
639 and permeability < 1 mD) with superimposed fracture-cave reservoirs (porosity > 6%
640 and permeability > 5 mD), which underwent multistage diagenetic modification,
641 resulting in intense vertical and horizontal heterogeneity.
642 2. The hydrocarbon hosted in these reservoirs have varying fluid properties
643 without gravity differentiation, and display unpredictable production of oil, gas and

644 water.

645 3. Oil emplacement in stratigraphic traps occurred in the Early and Late
646 Paleozoic and was followed by reservoir tightening which likely happened before the
647 onset of the Cenozoic. Subsequently, the Neogene gas charge in these tight reservoirs
648 led to a complex unconventional fluid distribution and production.

649 4. Understanding these complex carbonate reservoirs and the distribution of the
650 "sweet spots" is important for exploration and development strategies in the Tarim
651 basin. Here, optimal extraction of hydrocarbon requires new unconventional methods
652 that would unlock production from the tight carbonate matrix reservoirs.

653

654 **Acknowledgments**

655 The authors thank Tarim Oil Company of data support and project research.
656 Comments provided by editors and reviewers of the manuscript are much appreciated
657 and were very helpful in improving the manuscript. We are grateful to Zhenyu Wang,
658 Yungang Ji, Zhiming Xu, Xinli Liu, Mingjin Cai, Feng Ma, Chuan Hai and Xinsheng
659 Li for their help. This study has been partly supported by National Natural Science
660 Foundation of China (Grant No. 41472103) and National Science and Technology
661 Major Project (Grant No. 2016ZX05004001).

662

663

REFERENCES CITED

Al-Ameri, A. T. Gamadi, 2019, Optimization of acid fracturing for a tight carbonate reservoir: Petroleum, In press, Available online.

Amann-Hildenbrand, A., A. Ghanizadeh, and B.M. Krooss, 2012, Transport properties of unconventional gas systems: Marine and Petroleum Geology, v.31, p.90-99.

Arthur, M.A., and D.R. Cole, 2014, Unconventional hydrocarbon resources: prospects and problems: Elements, v.10, p.257-264.

Bruna, P.O., Y. Guglielmi, J. Lamarche, M. Floquet, F. Fournier, J.P. Sizun, A. Gallois, L. Marié, C. Bertrand, and F. Hollender, 2013, Porosity gain and loss in unconventional reservoirs: Example of rock typing in Lower Cretaceous hemipelagic limestones, SE France (Provence): Marine and Petroleum Geology, v.48, p.186-205.

Burchette, T.P., 2012, Carbonate rocks and petroleum reservoirs: a geological perspective from the industry: Geological Society, London, Special Publications, 370, 17-37.

Cai, C.F., W.S. Hu, and R.H. Worden, 2001, Thermochemical sulphate reduction in Cambro-Ordovician carbonates in Central Tarim: Marine and Petroleum Geology, v.18, p.729-741.

Cai, C.F., K.K. Li, H.T. Li, and B.S. Zhang, 2008, Evidence for cross formational hot brine flow from integrated $^{87}Sr/^{86}Sr$, REE and fluid inclusions of the Ordovician veins in Central Tarim: Applied Geochemistry, v.23, p.2226-2235.

685 Cai, C.F., C.M. Zhang, L.L. Cai, G.H. Wu, L. Jiang, Z.M. Xu, K.K. Li, A.L. Ma, and
686 L.X. Chen, 2009, Origins of Paleozoic oils in the Tarim Basin: Evidence from
687 sulfur isotopes and biomarkers: Chemical Geology, v.268, p.197-210.
688 Cai, C.F., W.X. He, L. Jiang, K.K. Li, L. Xiang, and L.Q. Jia, 2014, Petrological and
689 geochemical constraints on porosity difference between Lower Triassic sour-
690 and sweet-gas carbonate reservoirs in the Sichuan Basin: Marine and Petroleum
691 Geology, v.56, p.34-50.
692 Cai, C.F., C.M. Zhang, R.H. Worden, T.K. Wang, H.X. Li, L. Jiang, S.Y. Huang, and
693 B.S. Zhang, 2015, Application of sulfur and carbon isotopes to oil-source rock
694 correlation: A case study from the Tazhong area, Tarim Basin, China: Organic
695 Geochemistry, v.83-84, p.140-152.
696 Cai, C.F., A. Amrani, R.H. Worden, Q.L. Xiao, T.K. Wang, Z. Gvirtzman, H.X. Li, W.
697 Said-Ahmad, and L.Q. Jia, 2016, Sulfur isotopic compositions of individual
698 organosulfur compounds and their genetic links in the Lower Paleozoic
699 petroleum pools of the Tarim Basin, NW China: Geochimica et Cosmochimica
700 Acta, v.182, p.88-108.
701 Chew, K.J., 2014, The future of oil: unconventional fossil fuels. Phil. Trans. R. Soc. A,
702 v.372: 20120324.
703 Choquette, P.W., and L.C. Pray, 1970, Geologic nomenclature and classification of
704 porosity in sedimentary carbonates: AAPG Bull., v.54, p.207-250.

Davies, G.R., and L.B. Smith, 2006, Structurally controlled hydrothermal dolomite reservoir facies: an overview: AAPG Bull., v.90, p.1641-1690.

Deng, S.G., Y. Wang, Y.Y. Hu, X.M. Ge, X.Q. He, 2013, Integrated petrophysical log characterization for tight carbonate reservoir effectiveness: A case study from the Longgang area, Sichuan Basin, China: Petroleum Science, v.10, p.336-346.

Ding, W.L., T.L. Fan, B.S. Yu, X.B. Huang, and C. Liu, 2012, Ordovician carbonate reservoir fracture characteristics and fracture distribution forecasting in the Tazhong area of Tarim Basin, Northwest China: Journal of Petroleum Science and Engineering, v.86-87, p.62-70.

Dong, Y.P., D.F. He, S.S. Sun, X.M. Liu, X.H. Zhou, F.F. Zhang, Z. Yang, B. Cheng, G.C. Zhao, and J.H. Li, 2018, Subduction and accretionary tectonics of the East Kunlun orogen, western segment of the Central China Orogenic System: Earth Sci. Rev. available on line.

Du, J.H., 2010, Oil and gas exploration of Cambrian-Ordovician carbonate in Tarim basin: Beijing：Petroleum Industry Press, p.1-174 (in Chinese).

Ehrenberg, S.N., O. Walderhaug, and K. Bjorlykke, 2012, Carbonate porosity creation by mesogenetic dissolution: Reality or illusion?: AAPG Bull., v.96, p.217-233.

Esteban, M., and C. Taberner, 2003, Secondary porosity development during late burial in carbonate reservoirs as a result of mixing and/or cooling of brines: Journal of Geochemical Exploration, v.78-79, p.355-359.

725 Gao, D., C.S. Lin, H.J. Yang, F.F. Zuo, Z.Z. Cai, L.J. Zhang, J.Y. Liu, and H. Li, 2014,
726 Microfacies and depositional environments of the Late Ordovician Lianglitage
727 Formation at the Tazhong Uplift in the Tarim Basin of Northwest China: Journal
728 of Asian Earth Sciences, v.83, p.1-12.
729 Gao, Z.Q., and T.L. Fan, 2015, Carbonate platform-margin architecture and its
730 influence on Cambrian-Ordovician reef-shoal development, Tarim Basin, NW
731 China. Marine and Petroleum Geology, v.68, p.291-306.
732 Garland, J., J. Neilson, S.E. Laubach, and K.J. Whidden, 2012, Advances in carbonate
733 exploration and reservoir analysis: Geological Society, London, Special
734 Publications, v.370, p.1-15.
735 Guo, C., D.Z. Chen, H.R. Qing, S.F. Dong, G.R. Li, D. Wang, Y.X. Qian, and C.G.
736 Liu, 2016, Multiple dolomitization and later hydrothermal alteration on the
737 Upper Cambrian-Lower Ordovician carbonates in the northern Tarim Basin,
738 China: Marine and Petroleum Geology, v.72, p.295-316.
739 Guo, J.C., J.C. Ren, S.B. Wang, C.C. Jie, and L.B. Gou, 2019, Comprehensive study
740 of fracture flow characteristic and feasibility of hybrid volume stimulation
741 technique in tight fractured carbonate gas reservoir: Journal of Petroleum
742 Science and Engineering, v.174, p.362-373.
743 Hakami, A., A. Al-Mubarak, K. Al-Ramadan, C. Kurison, and I. Leyva, 2016,
744 Characterization of carbonate mudrocks of the Jurassic Tuwaiq Mountain
745 Formation, Jafurah basin, Saudi Arabia: Implications for unconventional

reservoir potential evaluation: Journal of Natural Gas Science and Engineering, v.33, p.1149-1168.

He, L., L., Zhao, J.X., Li, Ma, J., R.L., Liu, S.Q., Wang, and W.Q., Zhao, 2014, Complex relationship between porosity and permeability of carbonate reservoirs and its controlling factors: A case of platform facies in Pre-Caspian Basin: Petroleum Exploration and Development, v.41, p.206-214.

Holditch, S.A., 2006, Tight gas sands: SPE 103356, v.58, p.86-93.

Hosseini, M., V. Tavakoli, and M. Nazemi, 2018, The effect of heterogeneity on NMR derived capillary pressure curves, case study of Dariyan tight carbonate reservoir in the central Persian Gulf: Journal of Petroleum Science and Engineering, v.171, p.1113-1122.

Islam, M.R., 2015, Overview of Reservoir Simulation of Unconventional Reservoirs: In: Islam, M.R., (Ed.), Unconventional Gas Reservoirs, Elsevier, Amsterdam, p. 487-547.

Javadpour, F., 2009, Nanopores and apparent permeability of gas flow in Mudrocks (Shales and siltstones): Journal of Canadian Petroleum Technology, v.48, p.16-21.

Jia, C.Z., 1997, Tectonic characteristics and petroleum, Tarim basin, China: Beijing：Geological Publishing House, p.29-261 (in Chinese).

Jia, L.Q., C.F. Cai, L. Jiang, L. Zhang, H.X. Li, and W. Zhang, 2016, Petrological and geochemical constraints on diagenesis and mesogenetic dissolution of the

767 Ordovician carbonate reservoirs in the Tazhong area, Tarim Basin, NW China:
768 Marine and Petroleum Geology, v.78, p.271-290.
769 Jiang, L., W. Pan, C.F. Cai, L.Q. Jia, L. Pan, T.K. Wang, H.X. Li, S.L. Chen, and Y.
770 Chen, 2015, Fluid mixing induced by hydrothermal activity in the Ordovician
771 carbonates in Tarim Basin, China: Geofluids, v.169, p.249-262.
772 Jiang, Z.X., S.G. Lin, X.Q. Pang, and J. Wang, 2006, The comparison of two types of
773 tight sand gas reservoir: Petroleum Geology & Experiment, v.28, p.201-214 (in
774 Chinese with English abstract).
775 Kuznetsov, V.G., 1997, Oil and gas in reef reservoirs in the former USSR: Petroleum
776 Geoscience, v.3, p.65-71.
777 Law, B.E., and J.B. Curtis, 2002, Introduction to unconventional petroleum systems:
778 AAPG Bulletin, v.86, p.1851-1852.
779 Li, B.N., H. Shen, S.L. Qu, D. Wang, and C. Liu, 2018, Tight carbonate reservoir
780 characterization based on the modified rock physics model: Journal of Applied
781 Geophysics, v.159, p.374-385.
782 Li, C.X., X.F. Wang, B.L. Li, and D.F. He, 2013, Paleozoic fault systems of the
783 Tazhong Uplift, Tarim Basin: Marine and Petroleum Geology, v.39, p.48-58.
784 Li, K.K., C.F. Cai, L.Q. Jia, Y. Gao, Z. Jiang, T.K. Wang, and L. Jiang, 2014, The role
785 of thermochemical sulfate reduction in the genesis of high-quality deep marine
786 reservoirs within the central Tarim Basin, western China: Arabian Journal of
787 Geosciences, v.8, p.1-14.

788 Li, H.X., and C.F. Cai, 2017, Origin and evolution of formation water from the
789 Ordovician carbonate reservoir in the Tazhong area, Tarim Basin, NW China:
790 Journal of Petroleum Science and Engineering, v.148, p.103-114.
791 Li, Q.M., G.H. Wu, X.Q. Pang, W.Q. Pan, C.S. Luo, C.L. Wang, X.S. Li, and B. Zhou,
792 2010, Hydrocarbon accumulation conditions of Ordovician carbonate in Tarim
793 Basin: Acta Geologica Sinica, v.84, p.1180-1194.
794 Li, S.M., A. Amrani, X.Q. Pang, H.J. Yang, W. Said-Ahmad, B.S. Zhang and Q.J.
795 Pang, 2015, Origin and quantitative source assessment of deep oils in the
796 Tazhong Uplift, Tarim Basin: Organic Geochemistry, v.78, p.1-22.
797 Liu, J.Q., Z. Li, J.C. Huang and Y. Liu, 2012, Distinct sedimentary environments and
798 their influences on carbonate reservoir evolution of the Lianglitage Formation in
799 the Tarim Basin, Northwest China: Sci. China: Earth Sci, v.55, p.1641-1655.
800 Liu, K.Y., B. Julien, B.S. Zhang, N. Zhang, X.S. Lu, S.B. Liu, H. Pang, Z. Li, and
801 X.W. Guo, 2013, Hydrocarbon charge history of the Tazhong Ordovician
802 reservoirs, Tarim Basin as revealed from an integrated fluid inclusion study:
803 Petroleum Exploration and Development, v.40, p.171-180.
804 Liu, R.L., N. Li, Q.F. Feng, C.H., and K.W. Wang, 2009, Application of the triple
805 porosity model in well–log effectiveness estimation of the carbonate reservoir in
806 Tarim oilfield: Journal of Petroleum Science and Engineering, v.68, p.40-46.
807 Moore, C.H., and W.J. Wade, 2013, Carbonate Reservoirs: Porosity and Diagenesis in
808 a Sequence Stratigraphic Framework, v.67, Newnes

809 Nelson, P.H., 2009, Pore-throat sizes in sandstones, tight sandstones, and shales:
810 AAPG Bulletin, v.93, p.329-340.
811 Neng, Y., H.J., Yang, and X.L. Deng, 2018, Structural patterns of fault damage zones
812 in carbonate rocks and their influences on petroleum accumulation in Tazhong
813 Paleo-uplift, Tarim Basin, NW China: Petroleum Exploration and Development,
814 v.45, p.43-54.
815 Ni, X.F., A.J. Shen, W.Q. Pan, R.H. Zhang, H.F. Yu, Y. Dong, Y.F. Zhu, and C.F.
816 Wang, 2013, Geological modeling of excellent fracture-vug carbonate reservoirs:
817 A case study of the Ordovician in the northern slope of Tazhong palaeouplift and
818 the southern area of Tabei slope, Tarim Basin, NW China: Petroleum Exploration
819 and Development, v.40, p.444-453.
820 Pan, W.Q. Y.F. Liu, J.A.D. Dickson, A.J. Shen, J. Han, Y. Ye, H.L. Gao, P. Guan, L.J.
821 Zhang, and X.P. Zheng, 2009, Characteristics and geological model of
822 hydrothermal karstification from Palaeozoic carbonate rocks, Tarim Basin，
823 China: Acta Sedimentologica Sinica, v.27, p.983-994 (in Chinese with English
824 abstract).
825 Pang, H., J.Q. Chen, X.Q. Pang, K.Y. Liu, and C.F. Xiang, 2012, Estimation of the
826 hydrocarbon loss through major tectonic events in the Tazhong area, Tarim
827 Basin, west China: Marine and Petroleum Geology, v.38, p.195-210.
828 Pang, H., J.Q. Chen, X.Q. Pang, K.Y. Liu, L.F. Liu, C.F. Xiang, and S.M. Li, 2013,
829 Analysis of secondary migration of hydrocarbons in the Ordovician carbonate

reservoirs in the Tazhong uplift, Tarim Basin, China: AAPG Bulletin, v.97, p.1765-1783.

Pang, X.Q., J.Q. Chen, S.M. Li, J.F. Chen and H. Pang, 2016, Evaluation method and application of the relative contribution of marine hydrocarbon source rocks in the Tarim basin: A case study from the Tazhong area: Marine and Petroleum Geology, v.77, p.1-18.

Pang, X.Q., C.Z. Jia, H. Pang, and H.J. Yang, 2018, Destruction of hydrocarbon reservoirs due to tectonic modifications: Conceptual models and quantitative evaluation on the Tarim Basin, China: Marine and Petroleum Geology, v.91, p.401-421.

Qiu, N.S., J. Chang, Y.H. Zuo, J.Y. Wang, and H.L. Li, 2012, Thermal evolution and maturation of lower Paleozoic source rocks in the Tarim Basin, northwest China: AAPG Bulletin, v.96, p.789-821.

Qu, H.Z., Z.Y. Wang, H.J. Yang, Y.F. Zhang, H.F. Yu, and X. Wang, 2013, Karstification of reef-bank facies carbonate and its control on pore distribution: A case study of Upper Ordovician Lianglitage Formation in eastern Tazhong area, Tarim Basin, NW China: Petroleum Exploration and Development, v.40, p.552-558.

Rashid, F., P.W.J. Glover, P. Lorinczi, R. Collier, and J. Lawrence, 2015, Porosity and permeability of tight carbonate reservoir rocks in the north of Iraq: Journal of Petroleum Science and Engineering, v.133, p.147-161.

Rashid, F., P.W.J. Glover, P. Lorinczi, D. Hussein and J.A. Lawrence, 2017, Microstructural controls on reservoir quality in tight oil carbonate reservoir rocks: Journal of Petroleum Science and Engineering, v.156, p.814-826.

Ray, D.S., D.S. A., Al-Shammeli, N.K. Verma, S. Matar, D. Groen, D.J. Ghislain, G. Laurent, L.M. Thierry, A. Waleed, 2012, Characterizing and modeling natural fracture networks in a tight carbonate reservoir in the Middle East: A methodology: Bulletin of the Geological Society of Malaysia, v.58, p.29-35.

Ronchi, P., A. Ortenzi, O. Borromeo, M. Claps, and W.G. Zempolich, 2010, Depositional setting and diagenetic processes and their impact on the reservoir quality in the late Visean–Bashkirian Kashagan carbonate platform (Pre-Caspian Basin, Kazakhstan): AAPG Bulletin, v.94, p.1313-1348.

Rong, H., Y.Q. Jiao, L.Q. Wu, R. Wang, Y. Gu, and X.M. Wang, 2013, Architecture and evolution of calciclastic marginal slope fans of the Ordovician carbonate platform in the Yijianfang outcrop of the Bachu area, west Tarim Basin: AAPG Bulletin, v.97, p.1657-1681.

Shanley, K.W., R.M. Cluff, and J.W. Robinson, 2004, Factors controlling prolific gas production from low-permeability sandstone reservoirs: AAPG Bulletin, v.88, p.1083-1121.

Shen, A.J., W.Z. Zhao, A.P. Hu, M. She, Y.N. Chen, and X.F. Wang, 2015, Major factors controlling the development of marine carbonate reservoirs: Petroleum Exploration and Development, v.42, p.597-608.

872 Sivey, J.P., and W.J. Lee, 2013, Applied well test interpretation: Society of Petroleum
873 Engineers.
874 Tian, F., X.R. Luo, and W. Zhang, 2019, Integrated geological-geophysical
875 characterizations of deeply buried fractured-vuggy carbonate reservoirs in
876 Ordovician strata, Tarim Basin: Marine and Petroleum Geology, v.99, p.292-309.
877 Tankersley, T.H., W. Narr, G.R. King, R.H. Camerlo, A. Zhumagulova, M. Skalinski,
878 and Y. Pan, 2010, Reservoir modeling to characterize dual porosity, Tengiz Field,
879 Republic Of Kazakhstan (Russian): SPE Caspian Carbonates Technology
880 Conference, Atyrau, Kazakhstan, SPE-139836.
881 Volery, C., E. Davaud, C. Durlet, B. Clavel, J. Charollais, and B. Caline, 2010,
882 Microporous and tight limestones in the Urgonian Formation (late Hauterivian to
883 early Aptian) of the French Jura Mountains: focus on the factors controlling the
884 formation of microporous facies: Sedimentary Geology, v.230, p.21-34.
885 Wan, Y.Z., Y.W. Liu, F.F. Chen, N.Y. Wu, an G.W. Hu, 2018, Numerical well test
886 model for caved carbonate reservoirs and its application in Tarim Basin, China:
887 Journal of Petroleum Science and Engineering, v.161, p.611-624.
888 Wang, Z.M., K.Z. Zhao, G.H. Wu, L.J. Zhang, Z.Y. Wang, C.S. Luo, and X.S. Li,
889 2007, Development characteristics of the Upper Ordovician series reef flat
890 reservoirs in Tazhong No.1 slope break and their main controlling factors: Oil &
891 Gas Geology, v.28, p.797-801(in Chinese with English abstract).

892 Wang, Z.M., C.F. Cai, H.X. Li, H.J. Yang, T.K. Wang, K. Zhang, L.Q. Jia, and K.
893 Chen, 2014, Origin of late charged gas and its effect on property of oils in the
894 Ordovician in Tazhong area: Journal of Petroleum Science and Engineering, v.122,
895 p.83-93.
896 Wang, Z.Y., W. Chen, D. Li, C.H. Sun, G.H. Wu, and X.S. Li, 2008, Analysis of main
897 controlling geologic factors on upper Ordovician platform margin reef reservoir of
898 Tazhong I slope-break zone of Tarim Basin: Science and Technology Consulting
899 Herald, v.4, p.64-65 (in Chinese with English abstract).
900 Walsh, M.P., and B.F. Towler, 1995, Method computes PVT properties for gas
901 condensates. Oil and Gas Journal, v.93, p.83-86.
902 Wei, X.S., H.D. Chen, D.F. Zhang, R. Dai, Y.R. Guo, J.P. Chen, J.F. Ren, N. Liu, S.S.
903 Luo, and J.X. Zhao, 2017, Gas exploration potential of tight carbonate reservoirs:
904 A case study of Ordovician Majiagou Formation in the eastern Yi-Shan slope,
905 Ordos Basin, NW China: Petroleum Exploration and Development, v.44,
906 p.347-357.
907 Wu, G.H., H.J. Yang, T.L. Qu, H.W. Li, C.S. Luo, and B.L. Li, 2012, The fault system
908 characteristics and its controlling roles on marine carbonate hydrocarbon in the
909 Central uplift, Tarim Basin: Acta Petrologica Sinica, v.28, p.793-805 (in Chinese
910 with English abstract).

911 Wu, G.H., H.J. Yang, H.W. Li, and L.X. Sun, 2013, Controlling effects of the
912 Ordovician carbonate pore structure on hydrocarbon reservoirs in the Tarim Basin,
913 China: Petroleum Science, v.10, p.282-291.
914 Wu, G.H., X.Q. Pang, Q.M. Li, and H.J. Yang, 2016a, Structural characteristics in
915 intracratonic carbonate rocks and its implication for oil/gas accumulation: A case
916 study in the Tarim Basin, China: Beijing: Chinese Science Press (in Chinese).
917 Wu, G.H., H.J. Yang, S. He, S.J. Cao, X. Liu, and B. Jing, 2016b, Effects of structural
918 segmentation and faulting on carbonate reservoir properties: A case study from
919 the Central Uplift of the Tarim Basin, China: Marine and Petroleum Geology,
920 v.71, p.183-197.
921 Yang, H.J., G.H. Wu, J.F. Han, X.F. Wang, and Y.G. Ji, 2007, Characteristics of
922 hydrocarbon enrichment along the Ordovician carbonate platform margin in the
923 central uplift of Tarim Basin: Acta Petrolei Sinica, v.28, p. 26-30 (in Chinese with
924 English abstract).
925 Yang, H.J., K.K. Li, W.Q. Pan, Z.Y. Xiao, and C.F. Cai, 2012. Burial hydrothermal
926 dissolution fluid activity and its transforming effect on the reservoirs in
927 Ordovician in Central Tarim: Acta Petrologica Sinica, v.28, p.783-792 (in Chinese
928 with English abstract).
929 Yang, P., Z.D. Sun, X.H. Liang, H.Y. Li, and G.J. Dan, 2013, Seismic strategy for
930 predicting highly profitable wells in the fractured-vuggy carbonate reservoirs:
931 Petroleum Exploration and Development, v.40, p.537-541.

Yu, S., C.C. Pan, J.J. Wang, X.D. Jin, L.L. Jiang, D.Y. Liu, X.X. Lü, J.Z. Qin, Y.X. Qian, Y. Ding, and H.H. Chen, 2012, Correlation of crude oils and oil components from reservoirs and source rocks using carbon isotopic compositions of individual n-alkanes in the Tazhong and Tabei Uplift of the Tarim Basin, China: Organic Geochemistry, v.52, p.67-80.

Zhang, H., Z.X. Cai, L.X. Qi, and L. Yun, 2017, Diagenesis and origin of porosity formation of Upper Ordovician carbonate reservoir in northwestern Tazhong condensate field: Journal of Natural Gas Science and Engineering, v.38, p.139-158.

Zhang, S.C., B. Zhang, H.J. Yang, G.Y. Zhu, J. Su, and X. M. Wang, 2012, Adjustment and alteration of hydrocarbon reservoirs during the Late Himalayan Period, Tarim Basin, NW China: Petroleum Exploration and Development, v.39, p.712-724.

Zhang, S.C., H.P. Huang, J. Su, G.Y. Zhu, X.M. Wang, and S. Larter, 2014, Geochemistry of Paleozoic marine oils from the Tarim Basin, NW China. Part 4: Paleobiodegradation and oil charge mixing: Organic Geochemistry, v.67, p.41-57.

Zhang, Y.F., F. Tan, Y.B. Sun, W.Q. Pan, Z.Y. Wang, H.Q. Yang, and J.X. Zhao, 2018, Differences between reservoirs in the intra-platform and platform margin reef-shoal complexes of the Upper Ordovician Lianglitag Formation in the

952 Tazhong oil field, NW China, and corresponding exploration strategies: Marine
953 and Petroleum Geology, v.98, p.66-78.
954 Zhou, X. Y., X. Q. Pang, Q. M. Li, H. Pang, C.F. Xiang, Z.X. Jiang, S.M. Li, and L.F.
955 Liu, 2010, Advances and problems in hydrocarbon exploration in the Tazhong
956 area, Tarim Basin: Petroleum Science, v.7, p.164-178.
957 Zhu, G.Y., B.T. Zhang, H.J. Yang, J. Su, K.Y. Liu, and Y.F. Zhu, 2014, Secondary
958 alteration to ancient oil reservoirs by late gas filling in the Tazhong area, Tarim
959 Basin: Journal of Petroleum Science and Engineering, v.122, p.240-256.
960 Zou, C.N., G.Y. Zhang, S. Z. Tao, S.Y. Hu, X.D. Li, J.Z. Li, D.Z. Dong, R.K. Zhu,
961 X.J. Yuan, L.H. Hou, H. Qu, X. Zhao, J.H. Jia, X.H. Gao, Q.L. Guo, L.Wang,
962 and X.J. Li, 2010, Geological features, major discoveries and unconventional
963 petroleum geology in the global: Petroleum Exploration and Development, v.37,
964 p.129-145.
965 Zou, C.N., G.S. Zhang, Z. Yang, S.Z. Tao, L.H. Hou, R.K. Zhu, X.J. Yuan, Q.Q. Ran,
966 D.H. Li, and Z.P. Wang, 2013, Concepts, characteristics, potential and
967 technology of unconventional hydrocarbons: On unconventional petroleum
968 geology: Petroleum Exploration and Development, v.40, p.413-428.
969
970
971
972
973

Figure 1 (A) Tectonic outline of the Ordovician carbonate top in the Central Uplift (schematic map showing the location of the Tarim Basin in China); (B) Geological profile across the Tarim basin (after Wu et al., 2016a; see Figure 1A for location).

Figure 2 The sketch model of the oil/gas reservoirs of the Upper Ordovician in TZ-Nº1 Gasfield (modified from Wu et al., 2016a).

Figure 3 The petroleum system of the Central Uplift (modified from Li et al., 2010; Wu et al., 2016a).

Figure 4 Photographs of the Upper Ordovician reef-shoal rocks in TZ-Nº1 Gasfield. (A) framestone of corals ; T72, 5062.75m, core; (B) framestone of stromatoporoid; T822, 5700.01m, core; (C) clotted limestone; T72, 5061.35m, core. (C) bryozoan in bafflestone; T62, 4720.55m, core; (D) graistones comprise of bioclasts and calcarenite, intragranular porosity in bryozoan; T54, 4719.54m, thin section; (E) grainstone with intragranular dissolution porosity; T621, 4872.40m, thin section; (F) oosparite; intergranular dissolution porosity, T30, 5019.98m.

Figure 5 The correlation of the upper reef-shoal reservoirs in T62 area (modified after Wu et al., 2016a).

995 **Figure 6** The isopach map (A) of reef-shoal complex of Lianglitage Formation and
996 seismic profiles (B and C) along TZ-Nº1 Gasfield. Figure 6A is the thickness isopach
997 showing the thickness variation between the platform margin and the inner platform of
998 the Lianglitage Formation (the methods is after Du, 2010; Wu et al., 2016b). Figure
999 6B and 6C showing the chaotic seismic reflection, mound configuration and thick
1000 strata of the carbonate platform margin of Lianglitage Formation.
1001
1002 **Figure 7** Photographs of Ordovician carbonate pores in TZ-Nº1 Gasfield. (A)
1003 dissolution pores and vugs, T826 5685.85m, core,; (B) dissolution pores and vugs
1004 along fractures, T242, 4501.5m, core; (C) open fractures and dissolution pores, T62,
1005 4894.5m, core; (D) intragranular dissolution pores in bryozoan clast, T54, 5757.83m,
1006 thin section; (E) TZ62, intragranular and intergranular dissolution pores, 4753.9m, thin
1007 section; (F) T62, intergranular dissolved vugs, 5360.5m, thin section; (H) fractures and
1008 intergranular dissolution pores along fractures, T62, 4738.4m, thin section; (I)
1009 dissolved pores, TZ62, 4753.54m, SEM; (J) logging image of a cave, T58; (K) The
1010 seismic section of spectral decomposition of the Lianglitage Formation (The long
1011 string of strong amplitude reflection showing “bead-shape” reflection, after Wu et al.,
1012 2016b).
1013
1014 **Figure 8** Porosity-permeability relation from the core plugs tests (A) and (B) logging
1015 interpretation in TZ-Nº1 Gasfield; (C) formation permeability from the DST data (see

text for the method).

Figure 9 (A) The seismic attribute clustering description of the matrix reservoirs and (B) cross section showing the platform margin of the Upper Ordovician carbonate in T62 area. The method is after Wu, 2016a. The green to red areas are better reef-shoal reservoirs; the pink area is good reservoir and the blue area is bad or non-reservoir; the "bead-shape" reflection under well base showing large fracture-cave reservoirs.

Figure 10 The gas/oil ratio, oil density and water production of Ordovician reservoirs in eastern TZ-Nº1 Gasfield.

Figure 11 The gas component along the eastern TZ-Nº1 Gasfield.

Figure 12 The typical PVT and ternary phase chart of well fluid composition in TZ-Nº1 Gasfield.

Figure 13 The production contrast between DST and after acid fracturing of the Upper Ordovician carbonate in TZ-Nº1 Gasfield.

Figure 14 The typical production curves of the Upper Ordovician carbonate in

TZ-Nº1 Gasfield.

Figure 15 The variable production of oil density, oil/gas ratio of a well during the pre-production in TZ-Nº1 Gasfield.

Figure 16 A sketch of diagenesis and porosity evolution of the Upper Ordovician carbonate in TZ-Nº1 Gasfield. The burial data is from a typical well in the central TZ-Nº1 Gasfield. The cementation stages are after Wang et al., 2007; Wang et al., 2008; Zhang et al., 2017. The fracturing stages are after Wu et al., 2012, 2016a; Ding et al., 2012. The dissolution stages are after Wang et al., 2008; Yang et al., 2011; Shen et al., 2012; Ni et al., 2013; Wu et al., 2016a; Zhang et al., 2017. The porosity evolution is referenced after Shen et al., 2012; Wu et al., 2016a.

Figure 17 The hydrocarbon accumulation and evolution model of the Upper Ordovician in TZ-Nº1 Gasfield.

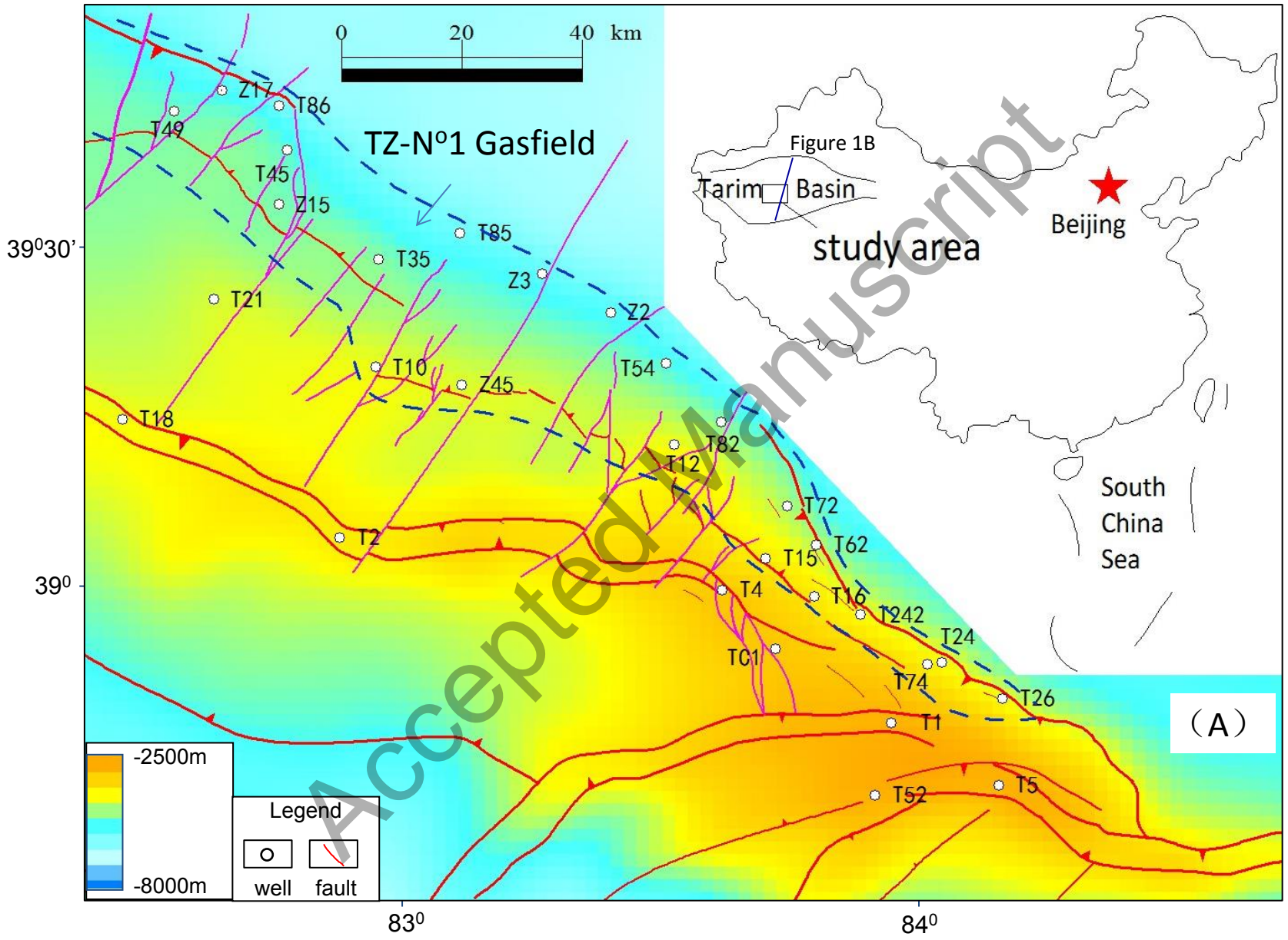

Fig. 1

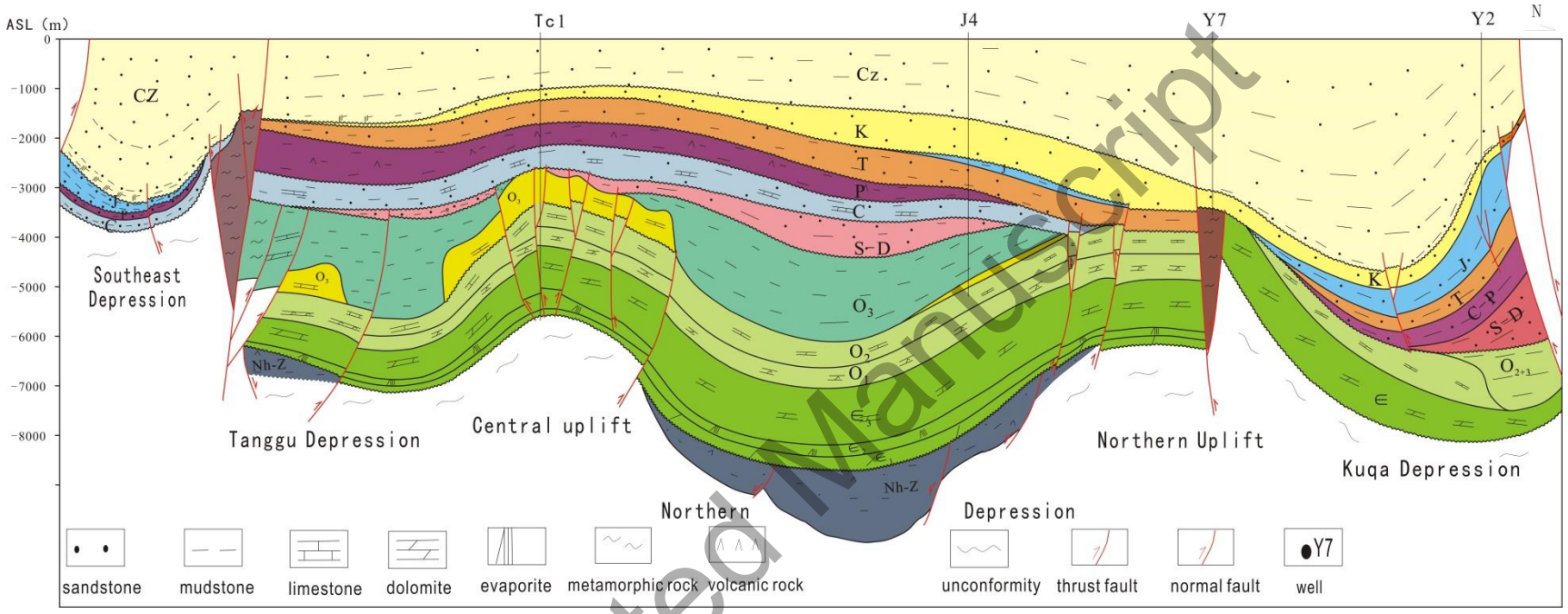

（B）

Figure 1

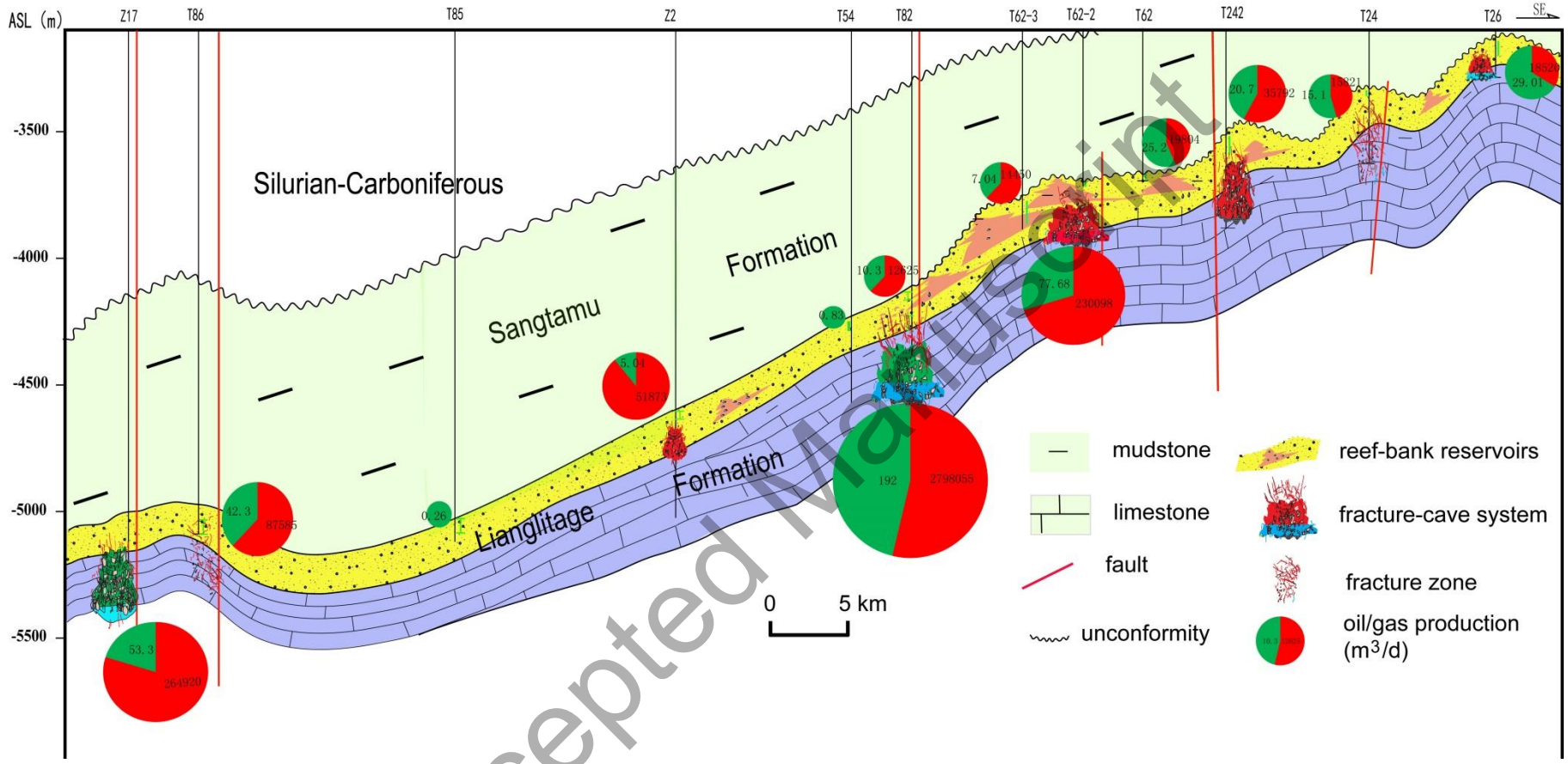

Figure 2

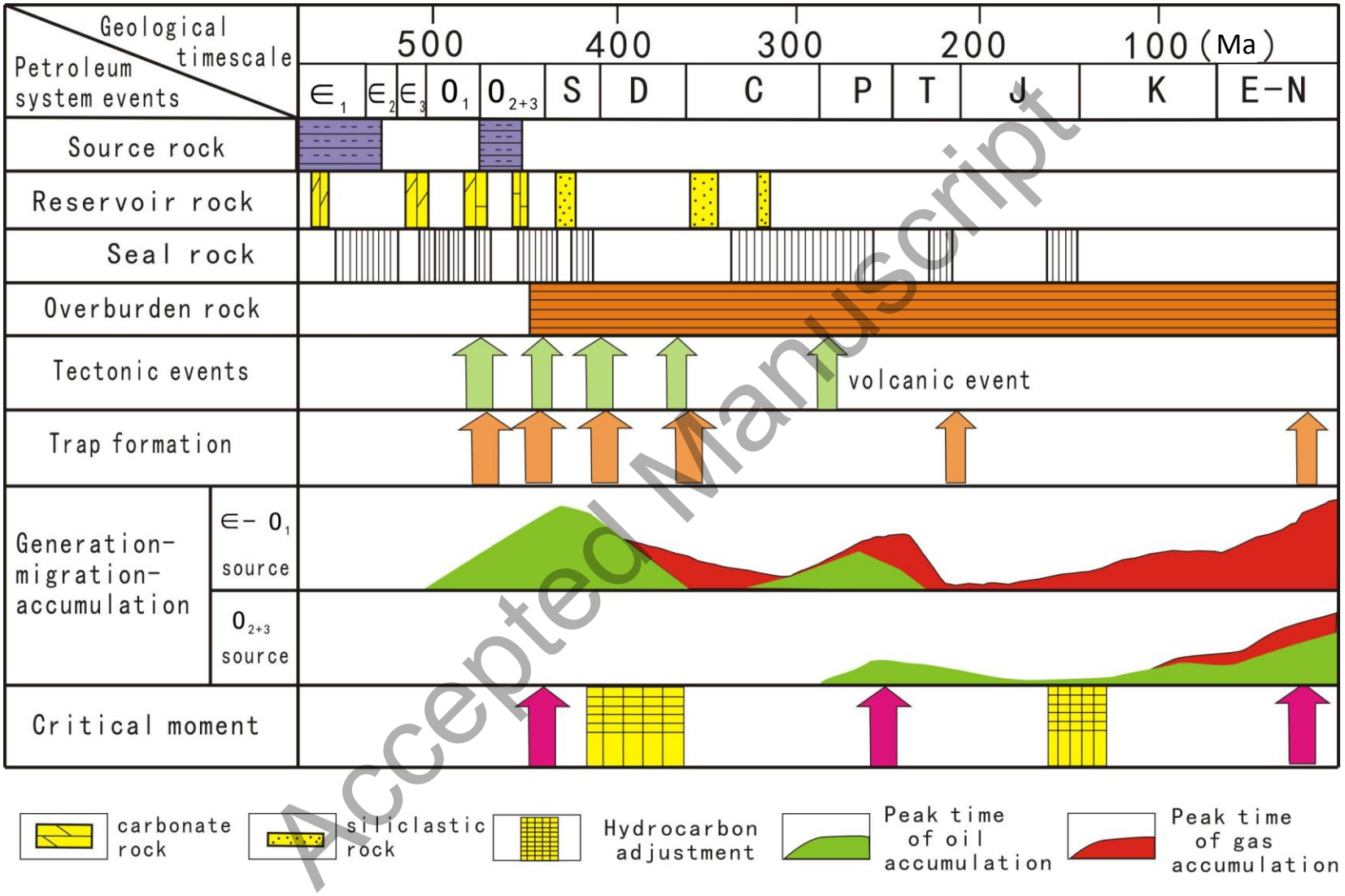

Figure 3

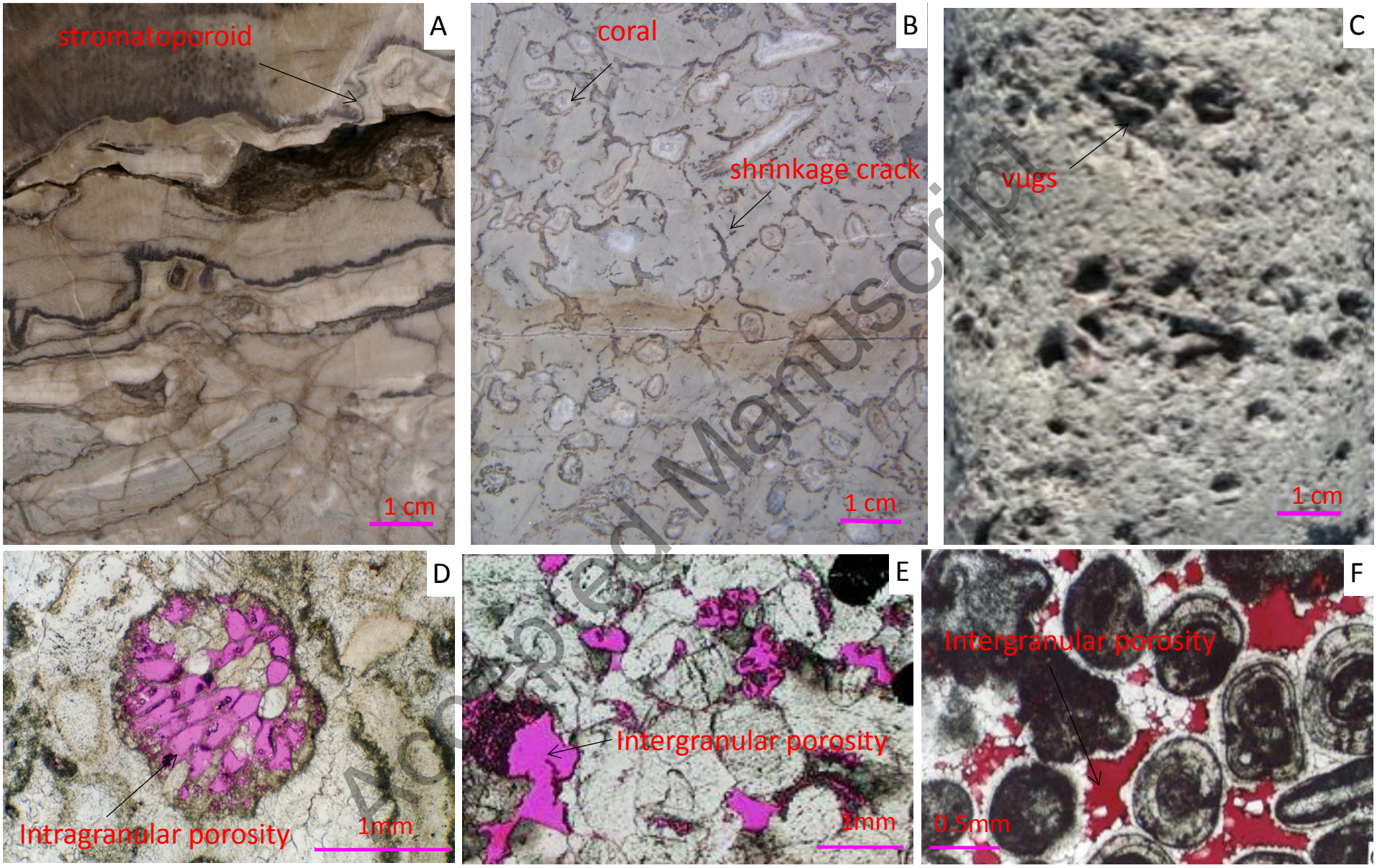

Figure 4

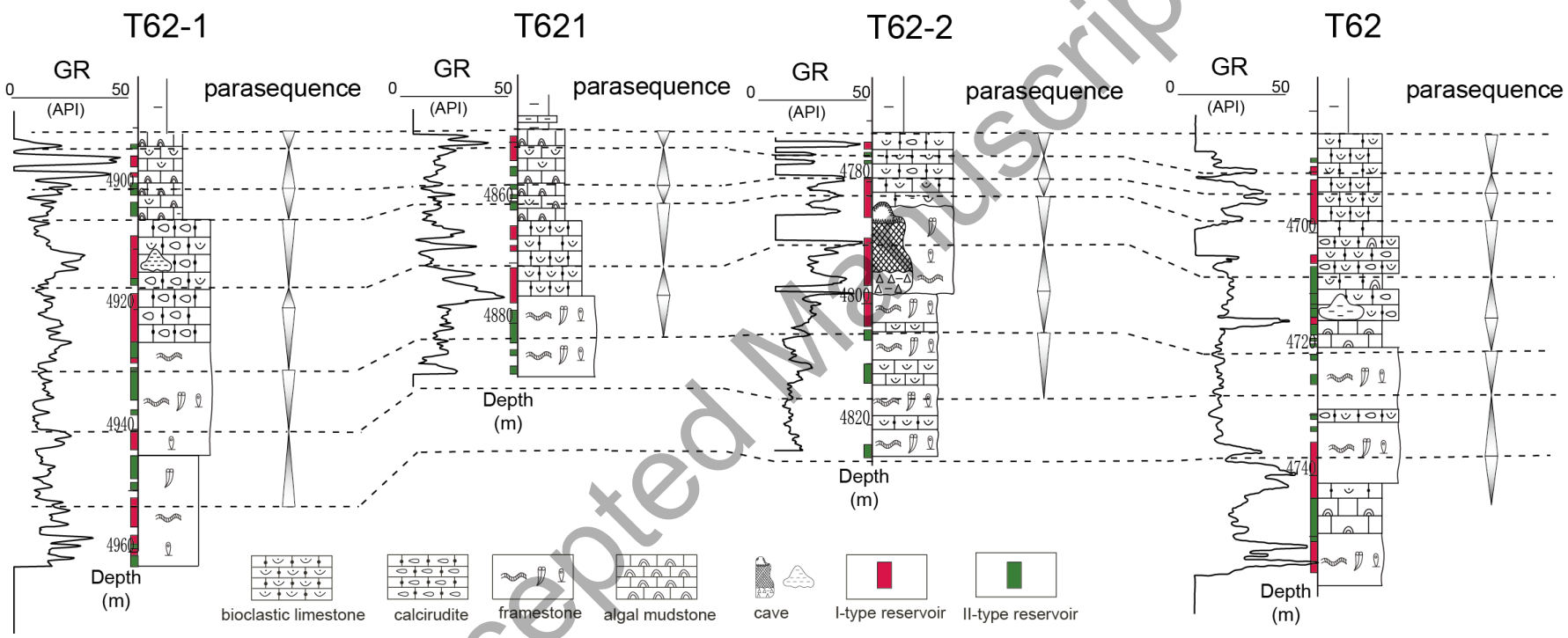

Figure 5

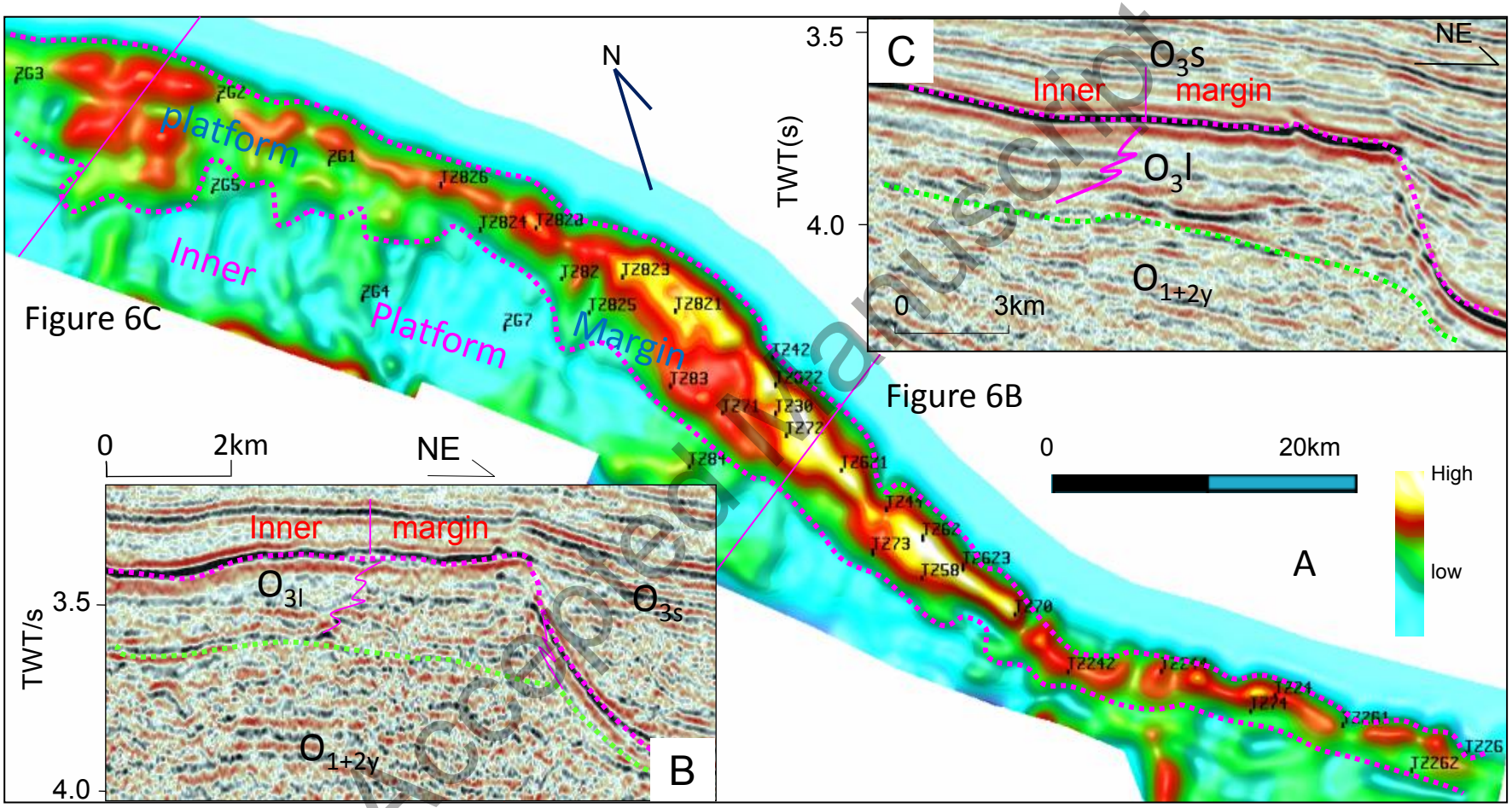

Figure 6

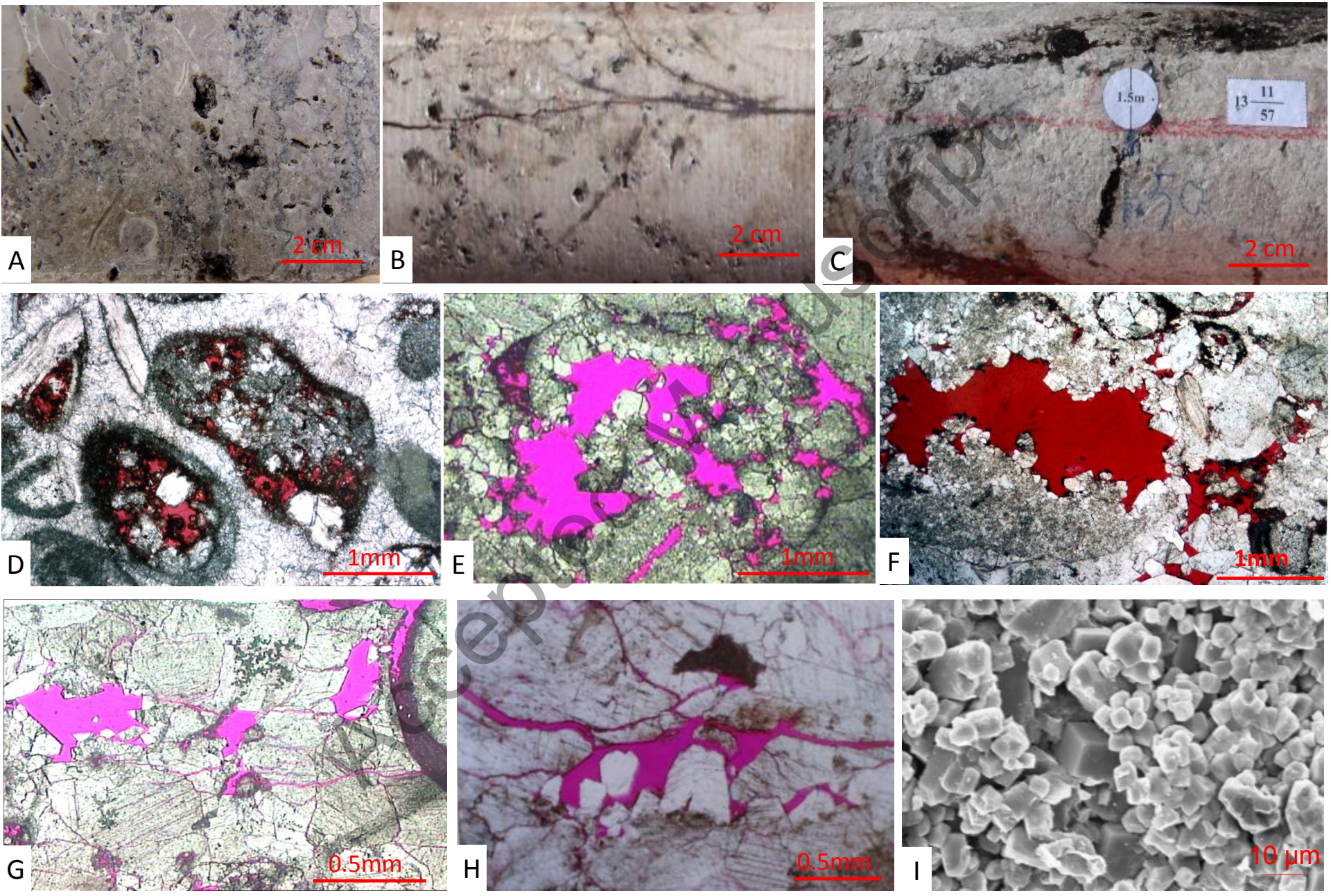

Figure 7

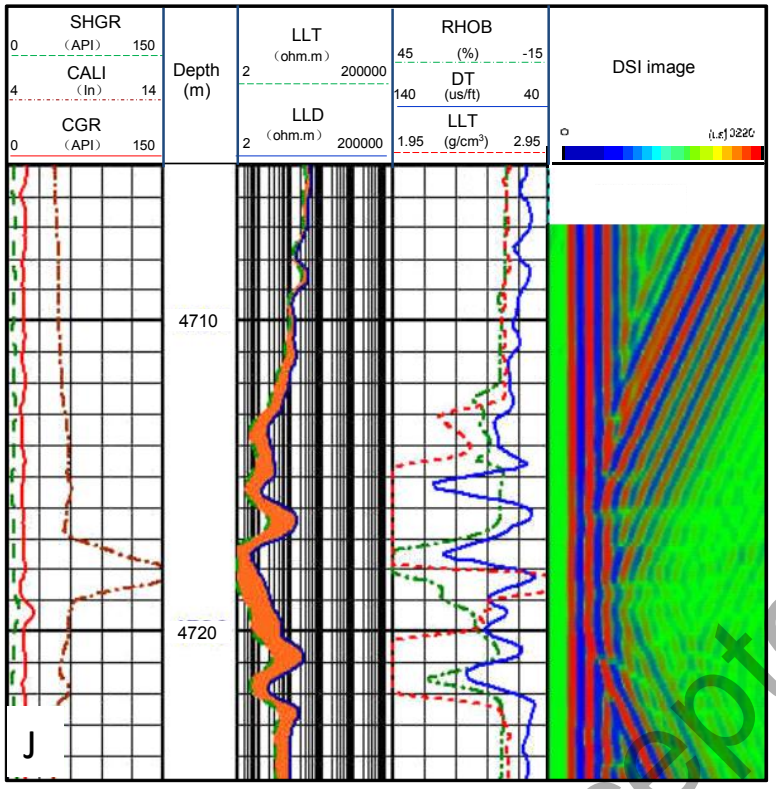

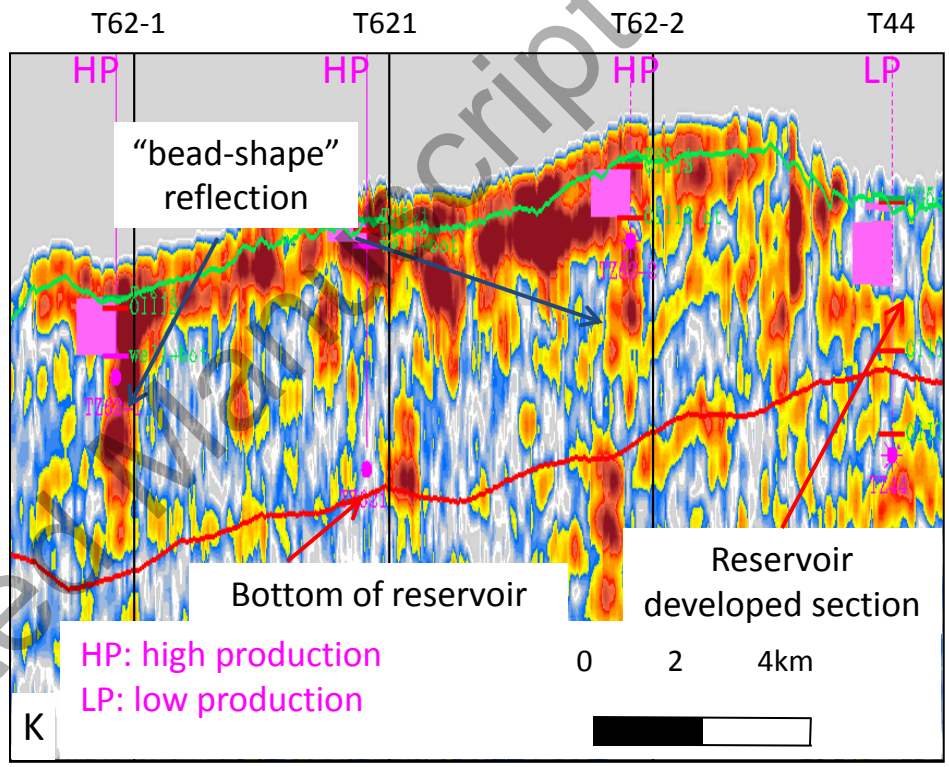

Figure 7

替换

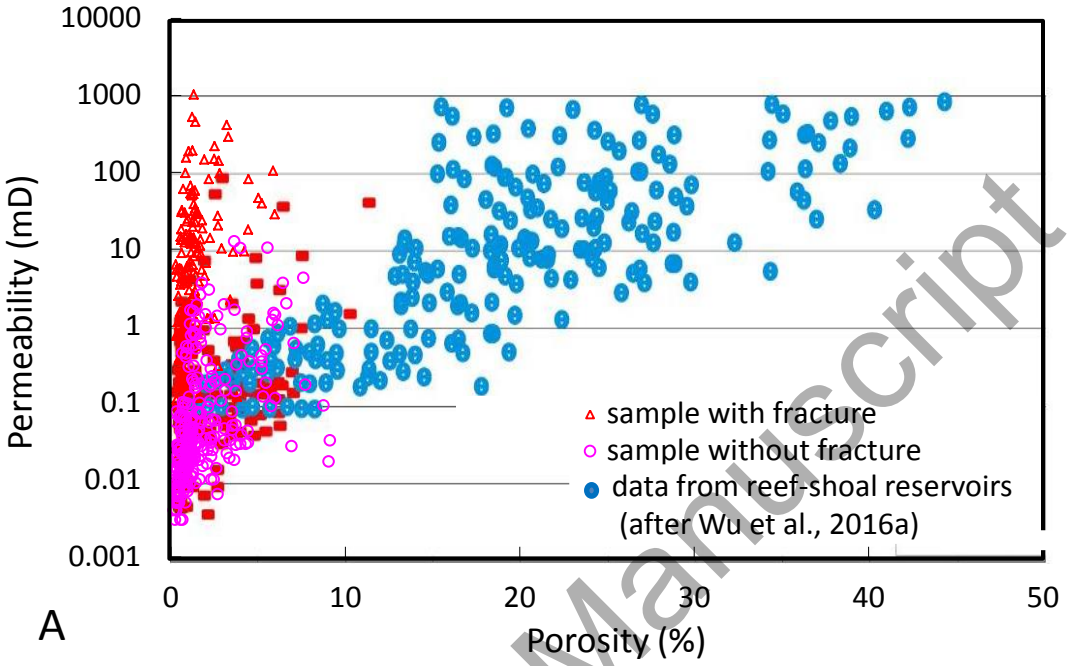

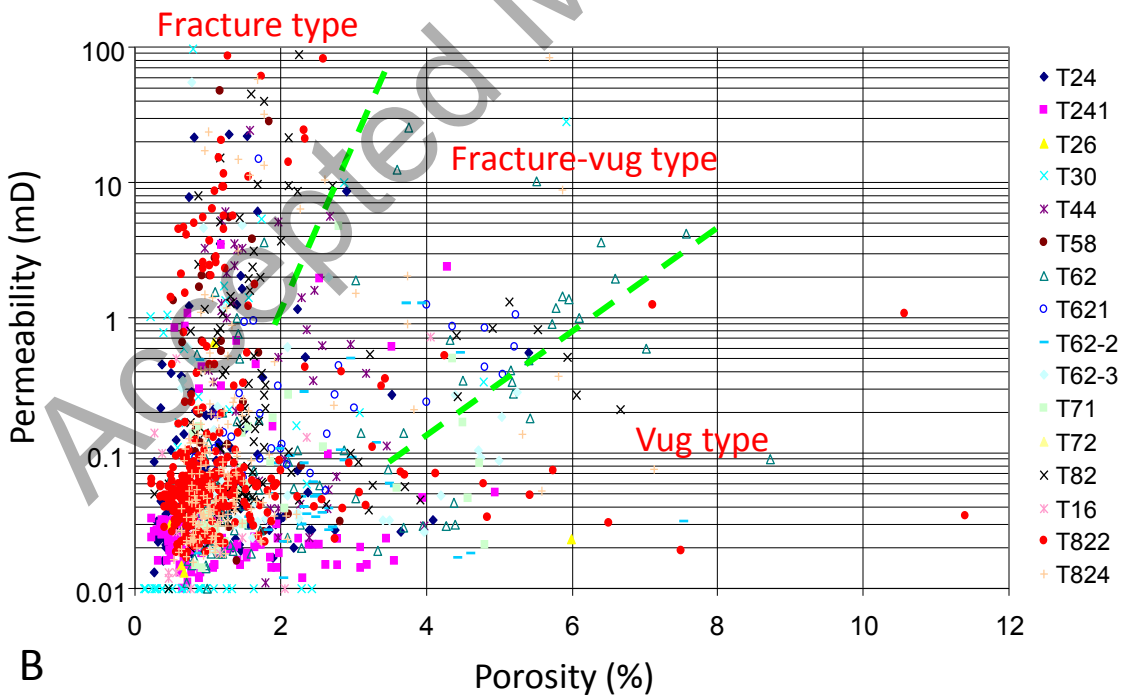

Figure 8

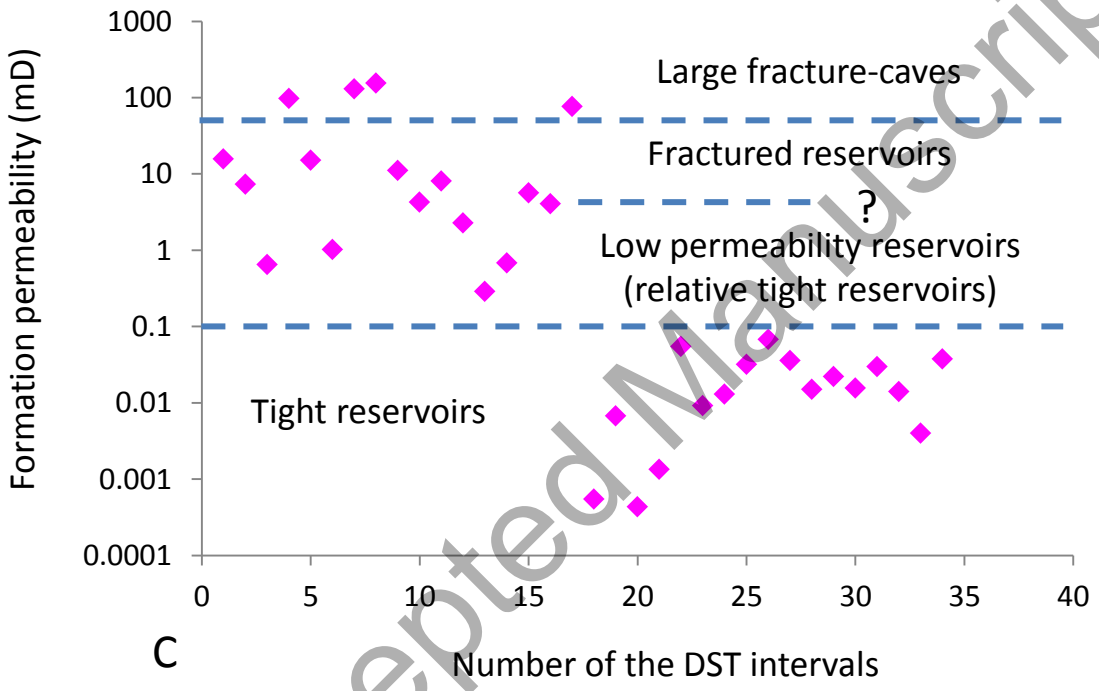

C

Figure 8

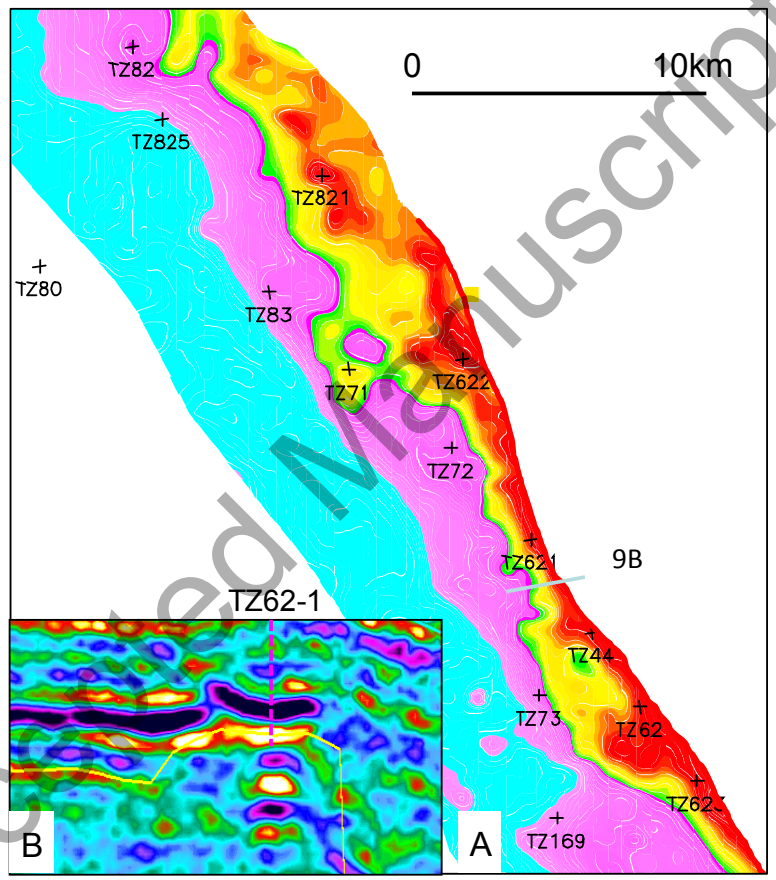

色棒

Figure 9

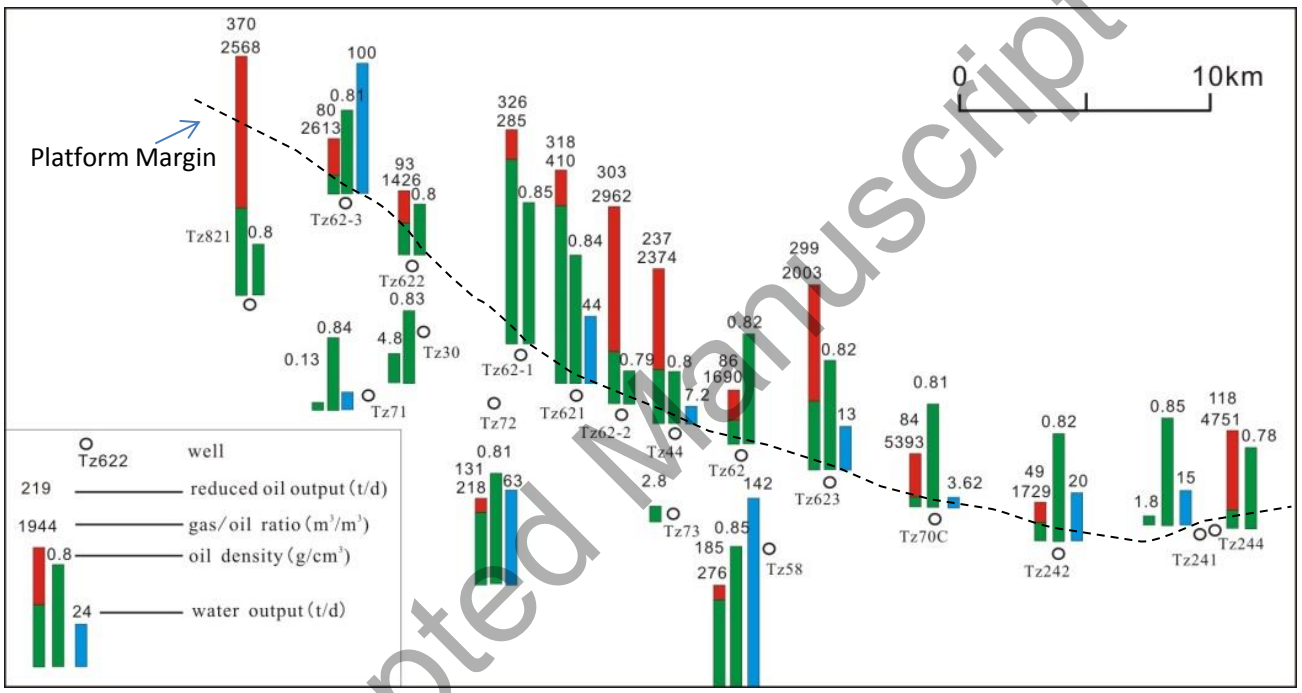

Output 换成production

Figure 10

t 换成bbl

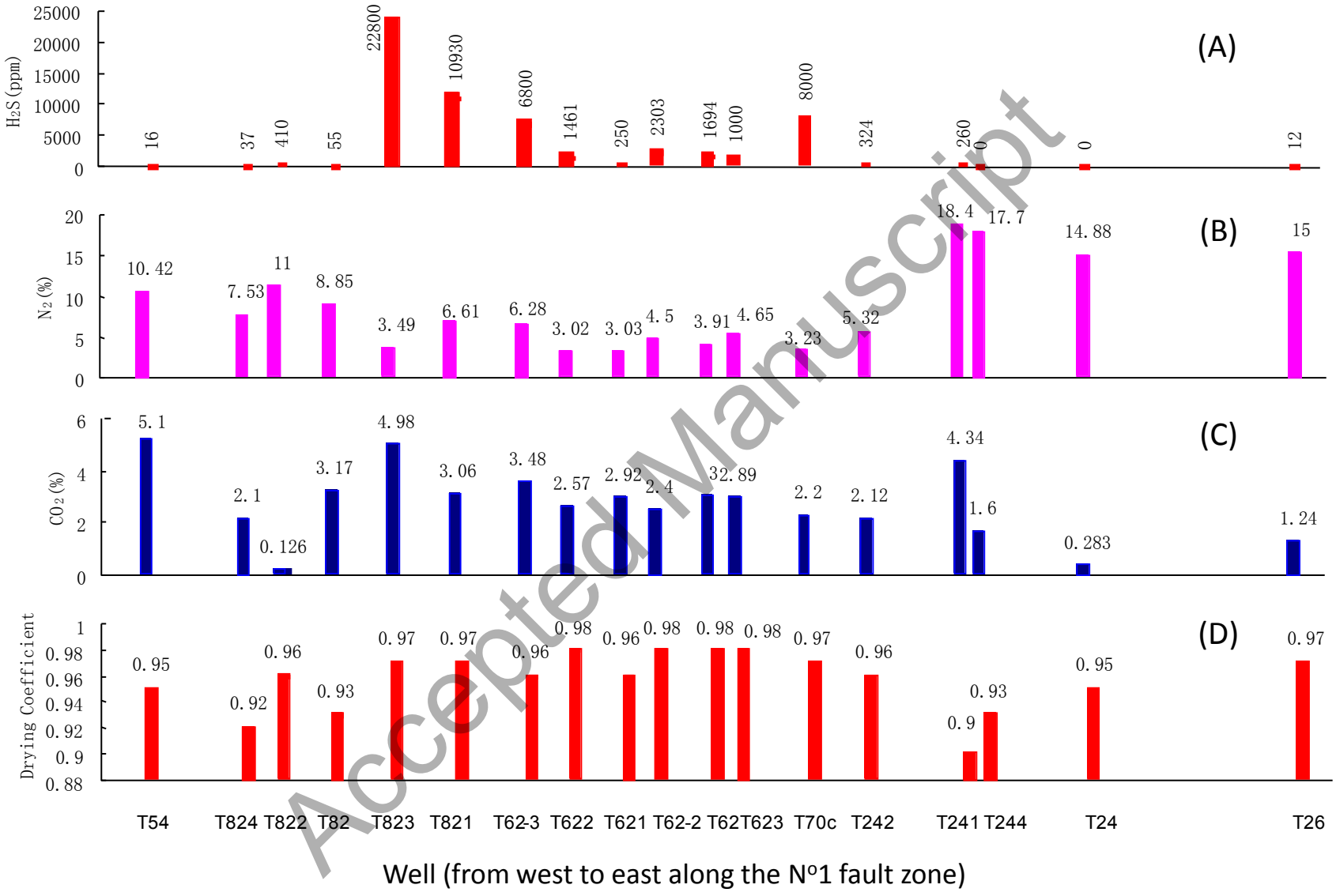

平面图四个杆

Figure 11

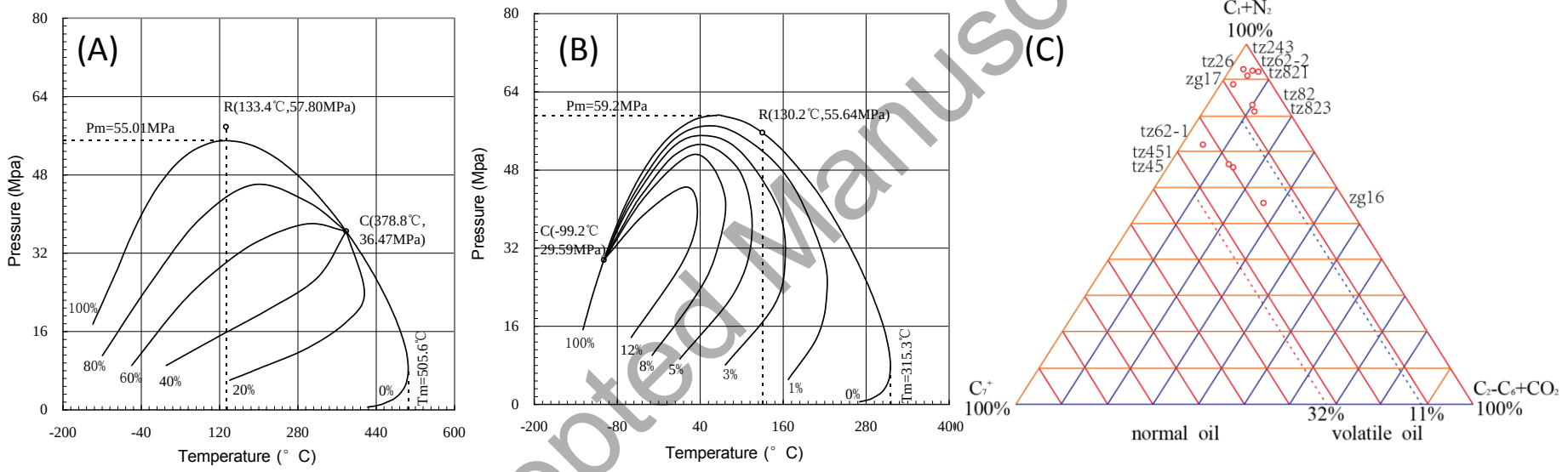

Figure 12

字体字号，不遮盖，井号清绘

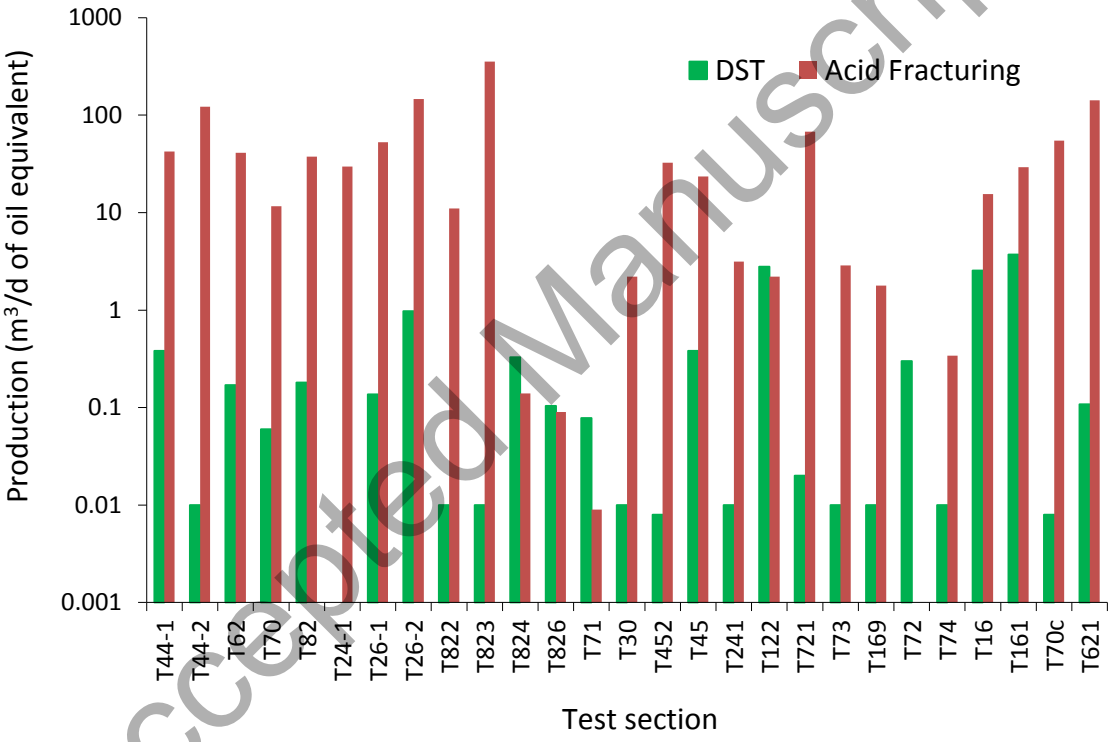

Figure 13

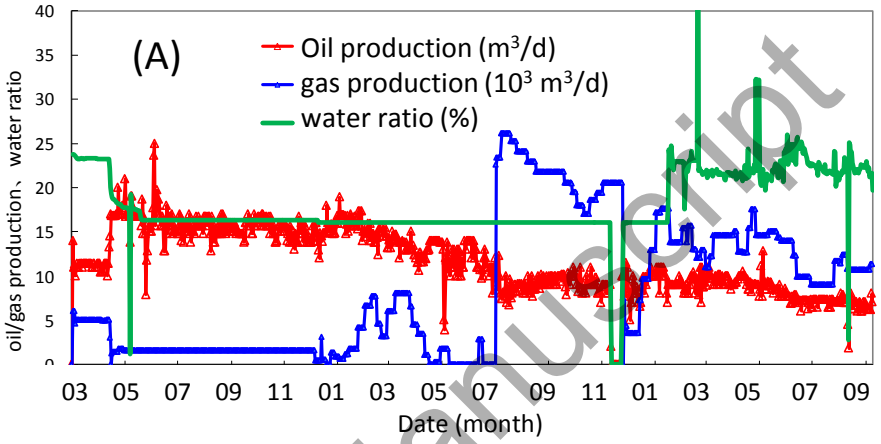

字号、大写首字母

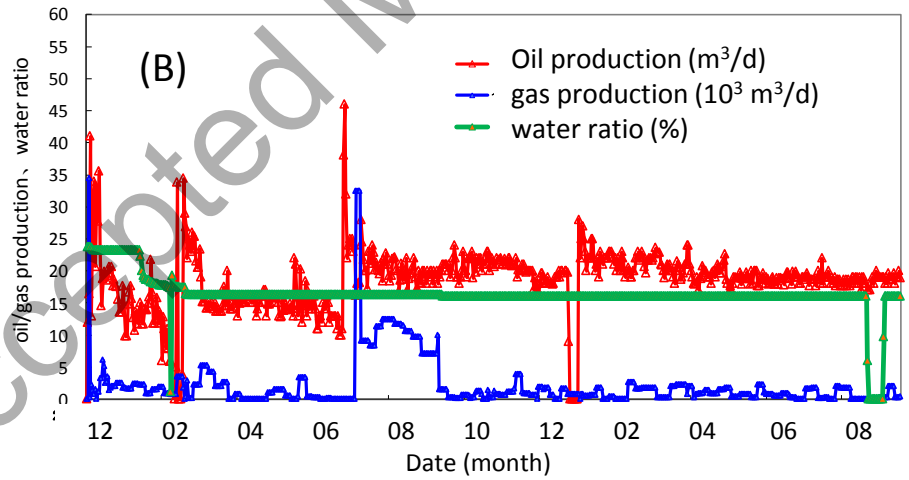

Figure 14

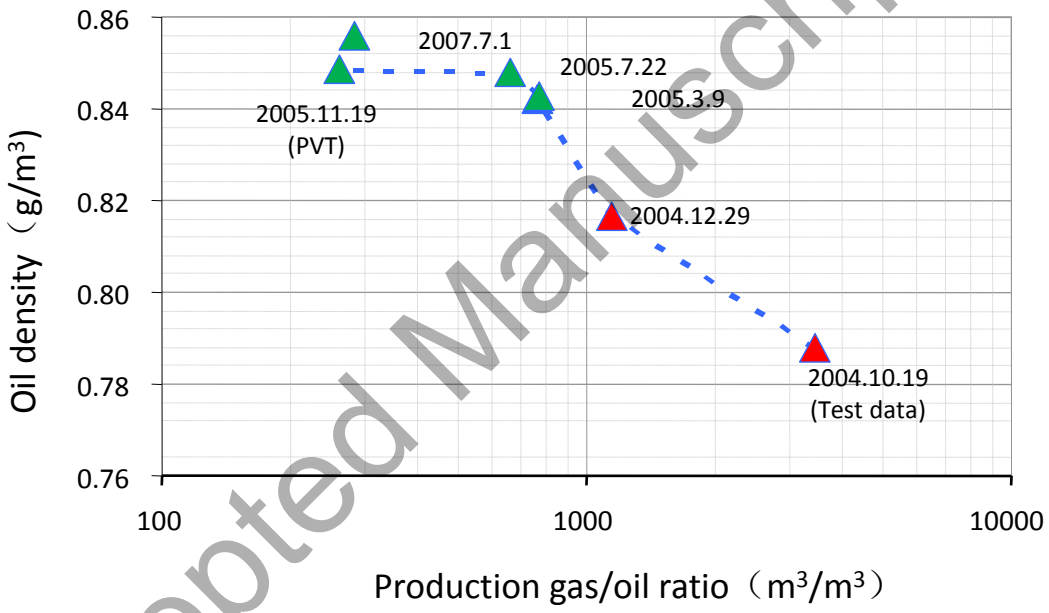

Figure 15

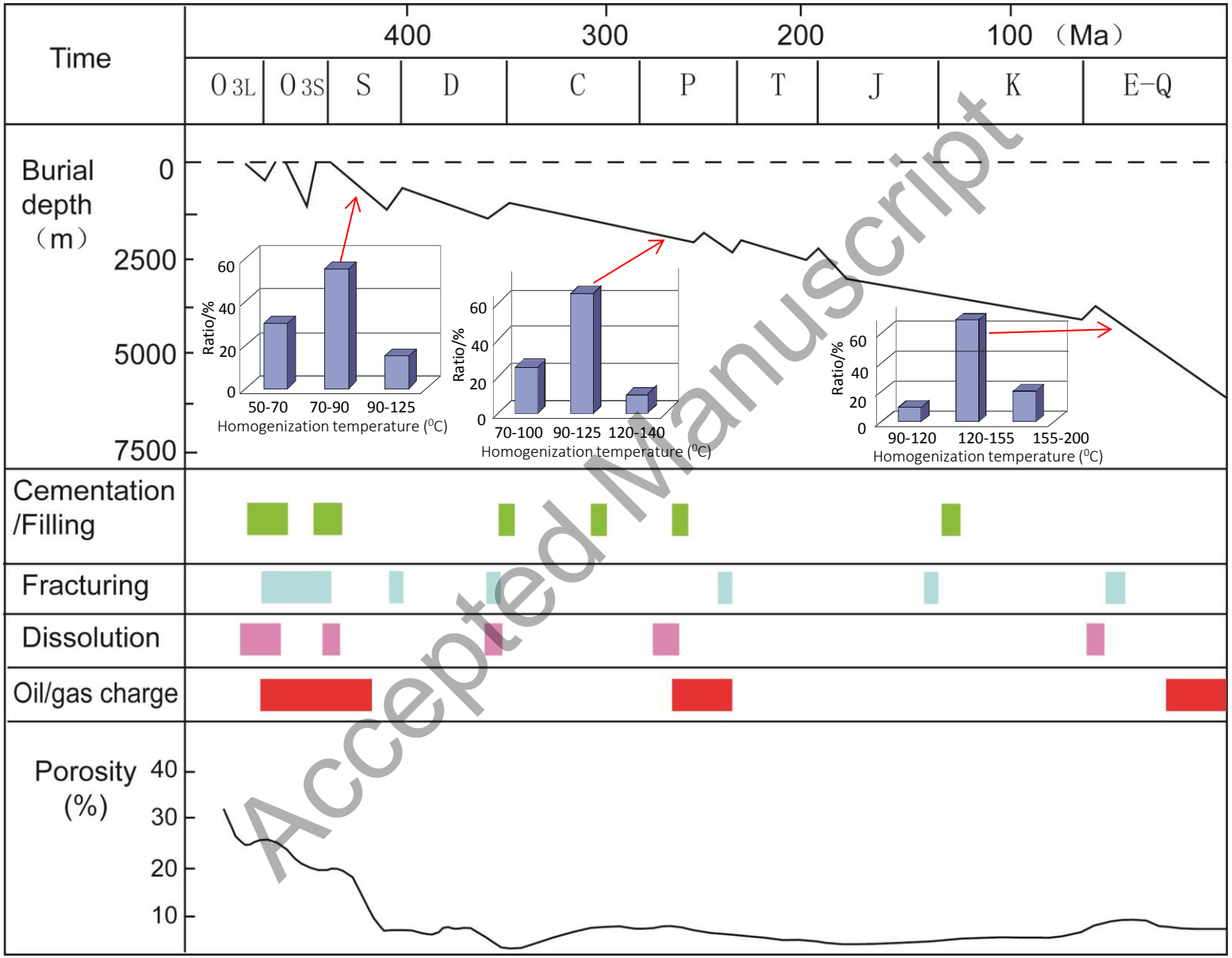

Figure 16

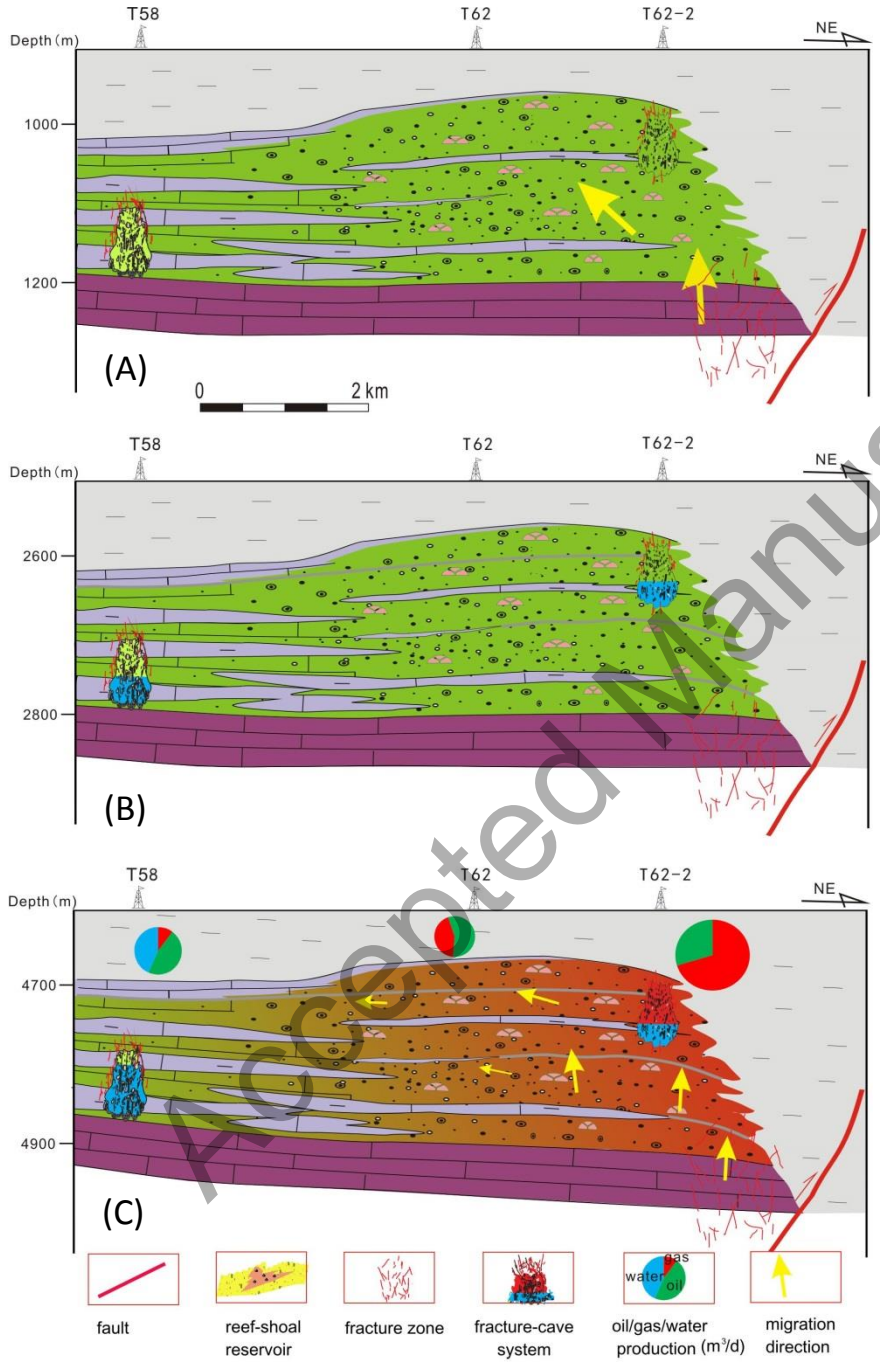

Figure 17